

ADA 029320

Research and Development Technical Report
ECOM-0115-F ✓

A.R.A.P. REPORT NO. 274, VOLUME I
VOICE COMMUNICATION VIA
SCATTERED ULTRAVIOLET RADIATION

FINAL REPORT

BY
E. STOKES FISHBURNE
MICHAEL E. NEER
GUIDO SANDRI

February 1976

Sponsored by

DEFENSE ADVANCED RESEARCH PROJECTS AGENCY
DARA ORDER NO. 2875

ECOM
UNITED STATES ARMY ELECTRONICS COMMAND
FORT MONMOUTH, NJ
CONTRACT DAMEP-75-C-0115
ASTRONOMICAL RESEARCH ASSOCIATES OF PRINCETON, INC.
381 WASHINGTON ROAD
PRINCETON, NJ



UNCLASSIFIED

SECURITY CLASSIFICATION OF THIS PAGE (When Data Entered)

REPORT DOCUMENTATION PAGE		READ INSTRUCTIONS BEFORE COMPLETING FORM
1. REPORT NUMBER	2. GOVT ACCESSION NO.	3. RECIPIENT CATALOG NUMBER (9)
4. TITLE (and Subtitle) VOICE COMMUNICATION VIA SCATTERED ULTRAVIOLET RADIATION Volume I.		5. TYPE OF REPORT & PERIOD COVERED FINAL REPORT 30 Dec 1974 - 29 Dec 1975
7. AUTHOR(s) E. STOKES FISHBURNE MICHAEL E. NEER GUIDO SANDRI		6. PERFORMING ORGANIZATION REPORT NUMBER A.R.A.P. REPORT NO. 274-I
8. PERFORMING ORGANIZATION NAME AND ADDRESS AERONAUTICAL RESEARCH ASSOCIATES OF PRINCETON, INC 50 WASHINGTON ROAD PRINCETON, N.J. 08540		8. CONTRACT OR GRANT NUMBER(s) DAAB07-75-C-0115 NEW
11. CONTROLLING OFFICE NAME AND ADDRESS ECOM UNITED STATES ARMY ELECTRONICS COMMAND FT. MONMOUTH, N.J. 07703		10. PROGRAM ELEMENT, PROJECT, TASK AREA & WORK UNIT NUMBERS ARPA Order 2875
14. MONITORING AGENCY NAME & ADDRESS (if different from Controlling Office) DEFENSE ADVANCED RESEARCH PROJECTS AGENCY 1400 WILSON BOULEVARD ARLINGTON, VIRGINIA 22209		12. REPORT DATE FEB 1976
15. SECURITY CLASS. (of this report) UNCLASSIFIED		13. NUMBER OF PAGES 82
16. DISTRIBUTION STATEMENT (of this Report) Approved for public release; distribution unlimited (14) ARAP-274-Vol-1		
17. DISTRIBUTION STATEMENT (of the abstract entered in block 20, if different from Report) (18) ECOM (19) 0115-F-1		
18. SUPPLEMENTARY NOTES		
19. KEY WORDS (Continue on reverse side if necessary and identify by block number) ULTRAVIOLET COMMUNICATION SCATTERING		
20. ABSTRACT (Continue on reverse side if necessary and identify by block number) A Nonline of sight voice communication has been accomplished in broad day- light via atmospheric scattering of ultraviolet radiation in the solar blind region of the spectrum. A frequency modulated high repetition rate hydrogen- xenon flashlamp is used for the transmitter and a combination of solar blind filters and photomultiplier tube is used for the receiver. An analysis is presented to show the potential for a practical, short range, all weather, secure, jam resistant communications system. An experimental study has been		

DD FORM 1473 1 JAN 73

EDITION OF 1 NOV 65 IS OBSOLETE

UNCLASSIFIED

SECURITY CLASSIFICATION OF THIS PAGE (When Data Entered)


008400

Y/B

UNCLASSIFIED

SECURITY CLASSIFICATION OF THIS PAGE(When Data Entered)

performed to systematically determine the scattering and absorption characteristics of ultraviolet light in the lower atmosphere, in both clear and rainy weather. A simplified atmospheric scattering theory has been developed which shows excellent agreement with the observed data. The theory utilizes the generalized Henyey-Greenstein phase function modified to resemble Deirmenjian's phase functions for polydispersed aerosols.



UNCLASSIFIED

SECURITY CLASSIFICATION OF THIS PAGE(When Data Entered)

TABLE OF CONTENTS

	<u>Page No.</u>
List of Illustrations	iv
List of Tables	vi
I. Introduction	1
II. Apparatus	6
III. Measurements	30
IV. Theoretical Investigation	55
V.* Voice Communication and Analysis	
VI.* Potential Applications of UV Voice Communication	
VII. Summary	74
VIII. References	76

*NOTE: Chapters V and VI have been classified CONFIDENTIAL and appear separately in Volume II of this report.

A. [illegible]	
15	White Section <input checked="" type="checkbox"/>
16	Black Section <input type="checkbox"/>
[illegible]	
BY [illegible]	
[illegible]	
[illegible]	
[illegible]	

LIST OF ILLUSTRATIONS

Figure

1. Variation of ozone density distribution with altitude.
2. Effect of ozone absorption on solar ultraviolet radiation incident on earth's surface.
3. Dependence of pulsed lamp spectral distribution on applied voltage.
4. Photographs of the UV sources employed for the scattering measurements (4a) and for the voice communication experiments (4b).
5. Basic electrical circuit for the high energy flashlamp.
6. Typical pulse profiles for high energy flashlamp.
7. High frequency trigger circuit for communication source.
8. Relative energy conversion of USSI bulbs.
9. Power response of 30 watt USSI bulb.
10. Transmittance curves of materials employed in solar blind systems.
11. Transmission characteristics of basic filters 1 and 2.
12. Transmission characteristics of 2680, 2580, and 2480 filters.
13. Overall system spectral response for the 2480, 2580, and 2680 filters.
14. Photograph of components of filter assembly.
15. Angular dependence of field of view function.
16. Measured quantum efficiency for EMR 542P-09-18 photomultiplier.
17. Photographs of the basic detecting system indicating pertinent components.
18. Apparatus employed to obtain field measurements of scattered radiation.
19. Signal processing - transmitter.

Figures (continued)

20. Signal processing - receiver.
21. Reduction of scattered light for measurement of attenuation coefficient.
22. Baum and Dunkelman attenuation data.
23. Geometry of atmospheric scattering measurements.
24. Atmospheric scattering footprints at .82 km.
25. Symmetry of scattering footprints with γ .
26. Scattering measurements for two different x locations.
27. Effects of reflecting additional light into vertical direction.
28. Geometry of blocking experiments.
29. Results of blocking experiments.
30. Rain enhancement of scattered radiation.
31. Scintillation measurements of solar background radiation.
32. Henyey-Greenstein phase functions.
33. Deirmendjian's phase functions.
34. Deirmendjian's haze types.
35. Comparison of various phase functions.
36. Circular volume elements.
37. Spherical volume elements.
38. General coordinate system.
39. Pulse arrival sequence.
40. Voice quality and background rejection.
41. Range aspect of UV secure communication.
42. Directionality aspect of UV secure communication.
43. Power required to jam UV system.

LIST OF TABLES

Table

1. Typical Results From Sky Survey.
2. Variation of Photon Count.
3. Estimated Range for Isotropic Transmission.
4. Background Rejection Using Photon Pairing.

I. INTRODUCTION

The objective of the research described in this report was to investigate the potential use of scattered ultraviolet radiation in the solar blind region of the spectrum, as a means of voice communication. A communication system using scattered UV light would utilize a frequency modulated, high repetition rate, UV flash lamp as a transmitter and a combination of solar blind filters and photomultiplier tube as a receiver. The voice communication could thus be accomplished day or night, bad weather or good, over hills, around corners or line of sight. The system would be inherently short range (due to ozone absorption), covert, secure, jam resistant, invisible to the eye and would not require a conventional antenna.

Virtually no sunlight reaches the earth's surface in the solar blind region of the spectrum (2200 to 2800Å) due to ozone absorption in the upper atmosphere. Consequently, an optical communication system can operate without interference from the sun in this spectral region. Typical distributions of ozone concentration as a function of altitude are given in Figure 1. It can be seen that the ozone concentration peaks at approximately 25 km and generally has a rather low value at sea level. The relatively low concentration of ozone at the earth's surface permits transmission of ultraviolet radiation over reasonable distances and, at the same time, has important implications with respect to security and antijamming characteristics.

Transmitted ultraviolet radiation undergoes strong Mie type scattering at low altitudes due to the high scattering cross-sections of atmospheric aerosols in this wavelength region. During periods of bad weather the concentration of atmospheric aerosols is likely to increase, thus enhancing the intensity of scattered radiation.

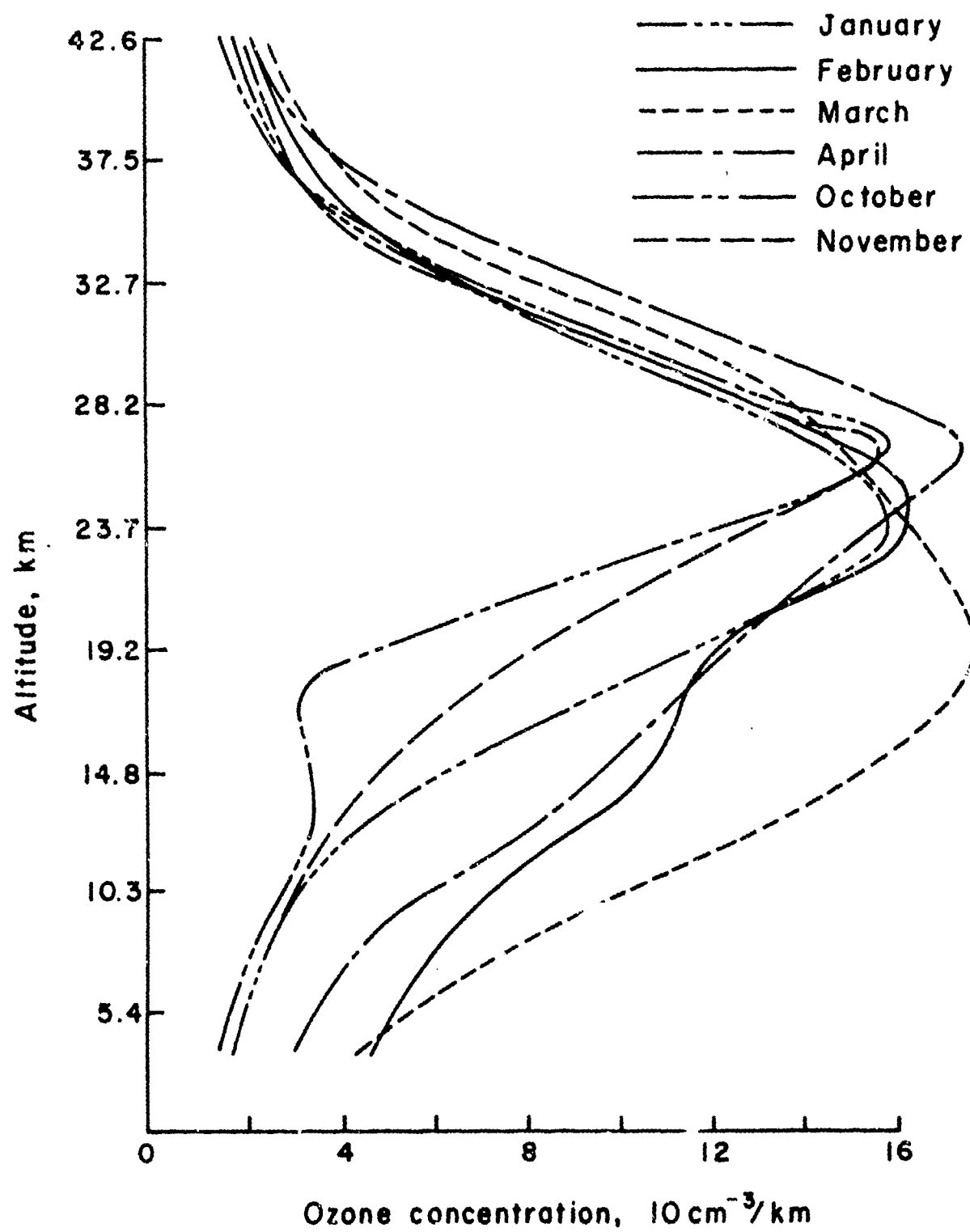


Figure 1. Variation of ozone density distribution with altitude.

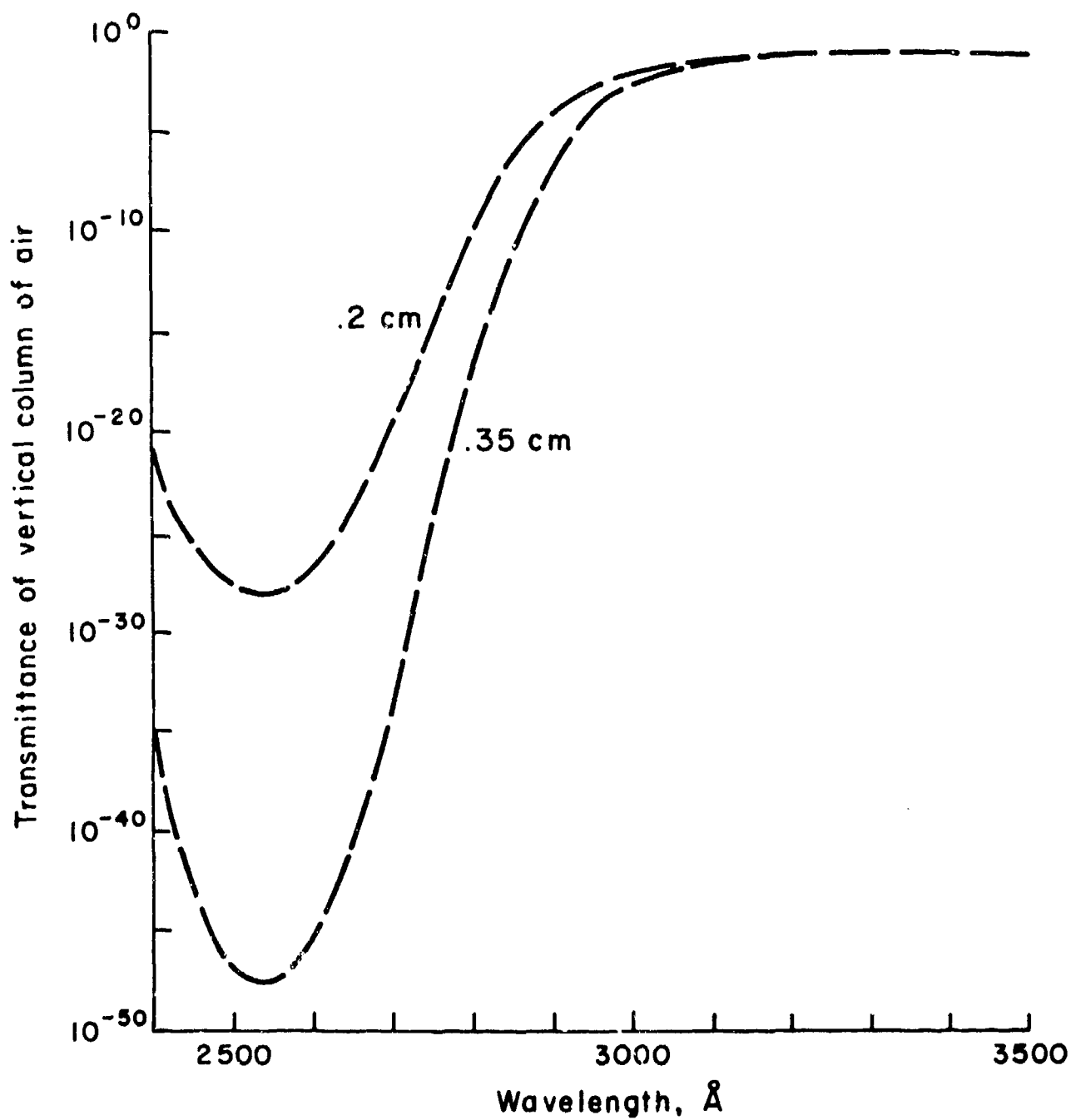


Figure 2. Effect of ozone absorption on solar ultraviolet radiation incident on Earth's surface.

It is through the scattering mechanism that transmitted UV light is able to travel over and around natural and manmade obstacles. The nature of the scattering process in the ultraviolet is therefore very important, primarily with respect to preferential scattering in the forward and backward direction. Unfortunately, virtually no fundamental scattering data are available for the solar blind region of the spectrum. An experimental and theoretical investigation of the manner in which the atmosphere processes a single flash of ultraviolet radiation from an isotropic source has therefore been undertaken as one of the major objectives of this study.

The individual goals of this investigation described in this report can be summarized as follows:

1. To determine the optimum components currently available for an ultraviolet communication system including solar blind filters, photo-multiplier tubes, high frequency UV flash-lamps, triggering circuits and other associated electronics.
2. To design and fabricate a proof-of-principle transmitter and receiver, over which voice communication can actually be accomplished via scattered ultraviolet radiation.
3. To test the efficiency of UV flashlamps in converting input power into UV energy, and to test the effects of various filter combinations and field of view effects on the received signal.
4. To determine experimentally the manner in which the atmosphere processes (scatters and absorbs) UV radiation.

5. To mathematically model the observed atmospheric scattering phenomena.
6. To combine the knowledge obtained from all of the above to make an estimate of the ultimate performance and power requirements of a practical UV communications sytem.
7. To outline the advantages and disadvantages of a UV communication system and to envision potential applications.

Finally, it is the purpose of this effort to identify the areas where further research needs to be carried out before a practical system can be developed.

II. APPARATUS

Ultraviolet Sources

Two types of ultraviolet sources were employed in the present study. Small bulbs with high pulse repetition rates were used in the investigation of voice communication. Large, high power flashlamps were used for obtaining measurements of atmospheric scattering. Both types of lamps generate ultraviolet radiation by passing electric arcs through hydrogen-xenon mixtures. Typical spectral distributions for these lamps are shown in Figure 3.

The high power flashlamps were obtained from the EG&G Company. These bulbs (FX-38C-3) have a maximum output power of 1000 joules per flash. A photograph of one of these lamps mounted on the triggering unit is shown in Figure 4a. Figure 4a does not show the large set of capacitors which are employed to provide the pulse energy to the flashlamp. The set contains three capacitors rated at 80 μF - 2000 V-DC and one capacitor rated at 200 μF - 2500 V-DC for a total rating of 440 μF .

Since the power of the flashlamps is $0.5 CV^2$ where C is the capacitance and V is the voltage, the power may be doubled by increasing the voltage by $\sqrt{2}$. Thus, voltages of 1414, 1000, 707, and 500 have been used for the atmospheric scattering studies. The basic electrical circuit for the flashlamp is shown in Figure 5. With this circuit the pulsewidth of the lamp, or the duration of the flash, is proportional to \sqrt{LC} where L is the circuit inductance. Typical pulse profiles are shown in Figure 6. For the 440 μF set of capacitors, the flashlamp produced a pulse of approximately 1 msec duration.

The high repetition rate bulbs were obtained from United States Scientific Instruments Inc. These bulbs were of two basic designs, one rated at 10 watts, the other at 30 watts. Both bulbs were successfully operated at 8000 cycles per second. The high frequency trigger circuit for these bulbs is shown in Figure 7. The 10 watt

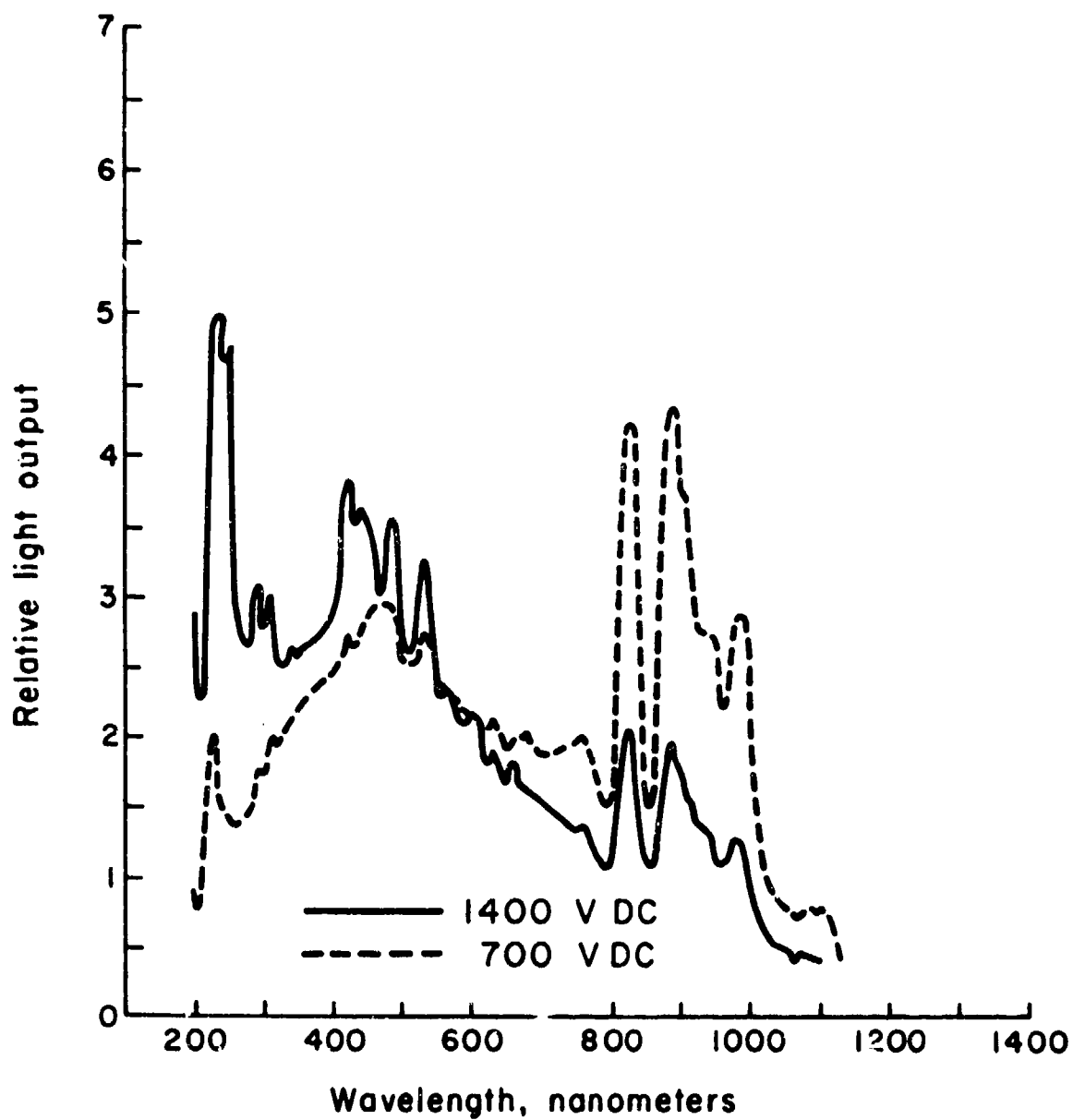
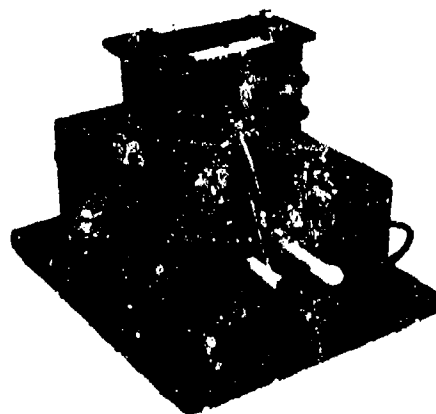
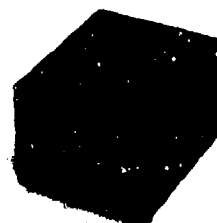


Figure 3. Dependence of pulsed lamp spectral distribution on applied voltage

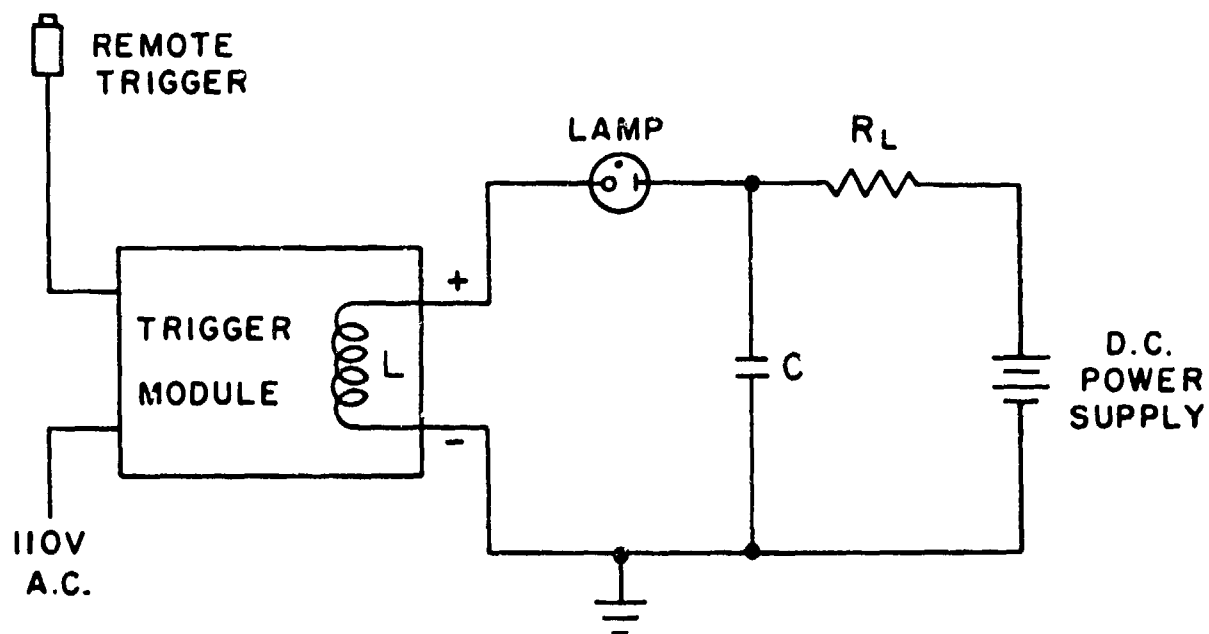


4a



4b

Figure 4. Photographs of the UV sources employed for the scattering measurements (4a) and for the voice communication experiments (4b).

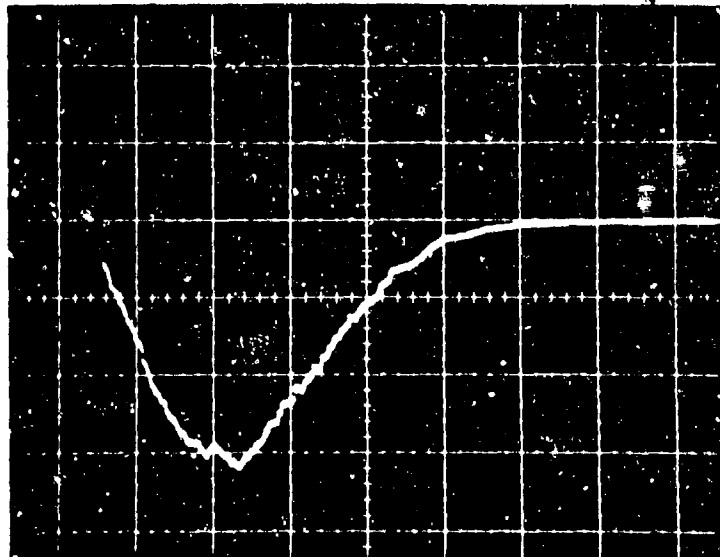


$$L = 280 \mu H$$

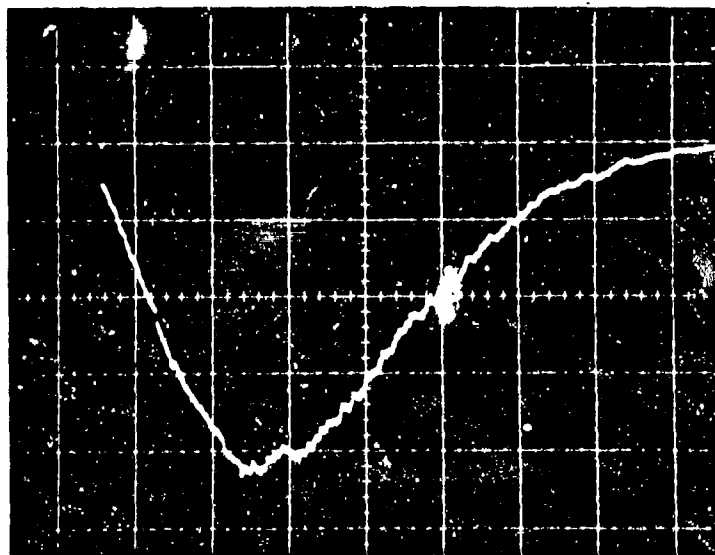
$$C = 440 \mu F$$

$$R_L = 0$$

Figure 5 Basic electrical circuit for the high energy flasulamp.



80 μ F



160 μ F

Figure 6. Typical pulse profiles for high energy flashlamp.

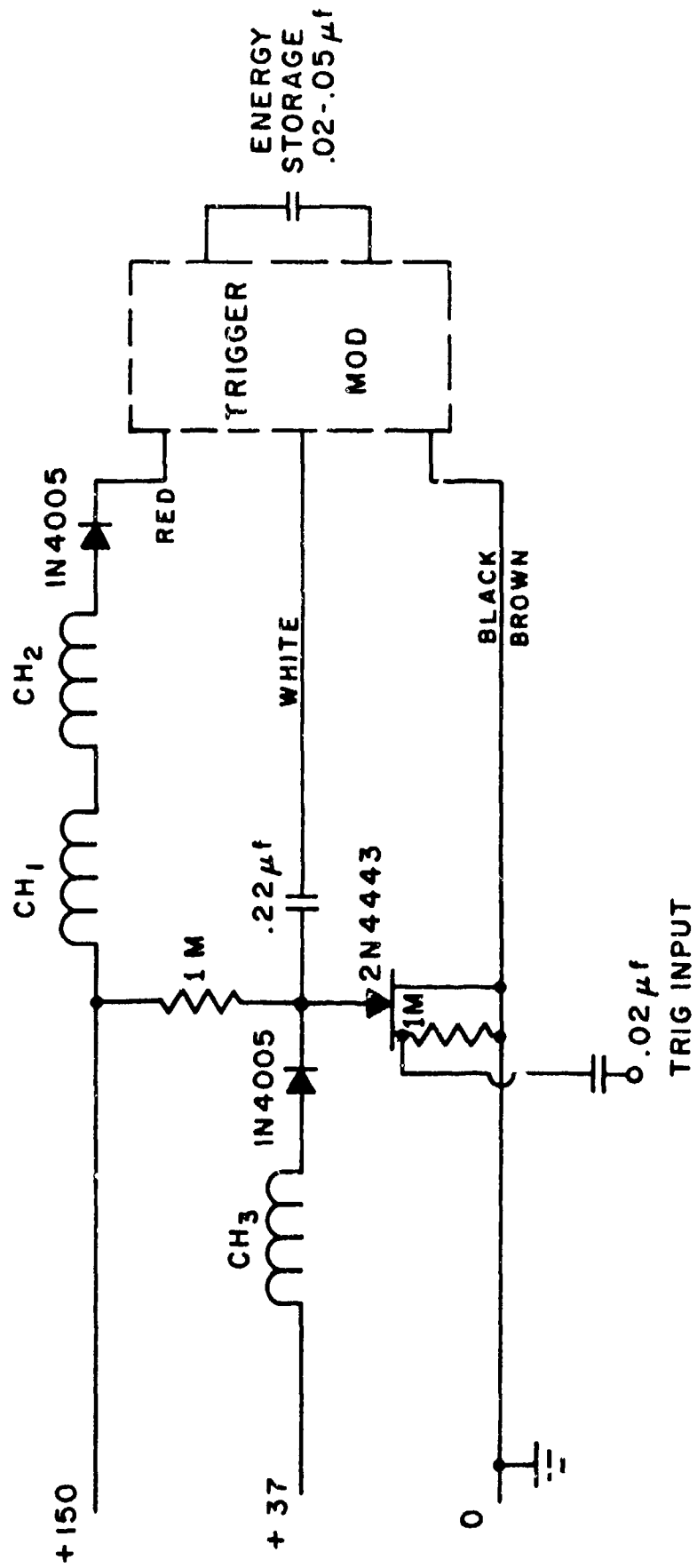


Figure 7. High frequency trigger circuit for communication source.

bulb is shown in Figure 4b mounted within a box containing the trigger circuit. The front surface of the lamp is made of Corning type 7-54 glass which does not transmit in the visible spectral region. The 30 watt bulb which is not shown has been mounted on top of the box shown in Figure 4b.

An experimental analysis of the two bulbs has been conducted to determine the relative UV output as a function of input power. It should be indicated at this point that the bulbs were designed for photocopying. Thus, the UV radiation has been intentionally suppressed. The results of our analysis are shown in Figures 8 and 9. As can be seen from the figures, enhancement of the UV radiation requires high voltage and low capacitance for a given power setting. The large increase in UV output with power is shown in Figure 9. As the input power is increased from 4 to 6 watts, the UV output increases by almost 300%. Unfortunately, the lamps and associated trigger circuitry were originally designed to achieve the rated power with high capacitance and low voltage which enhances the visible radiation used in photocopying. At voltages above 190V shorting occurs within the lamp circuitry thereby establishing an upper voltage limit. The power obtainable from A.R.A.P.'s 50 milli-amp DC power supply is consequently limited to less than 10 watts of average power. A conversion efficiency of input power to UV output of approximately .1% has been measured at the highest power setting shown in Figure 9.

Filters

The type of filters necessary to provide the required long wavelength solar radiation rejection are quite unique. Historically, the filters have been composed of numerous substances such as nickel sulphate hexahydrate, cation-x, Corning glass 9863, and aluminum interference filters. The various transmittances of these materials and several combinations are shown in Figure 10. The basic problems with these filters are the low peak transmittance, 3-5%, and the size, minimum 1.5-inches total depth. These filters currently are

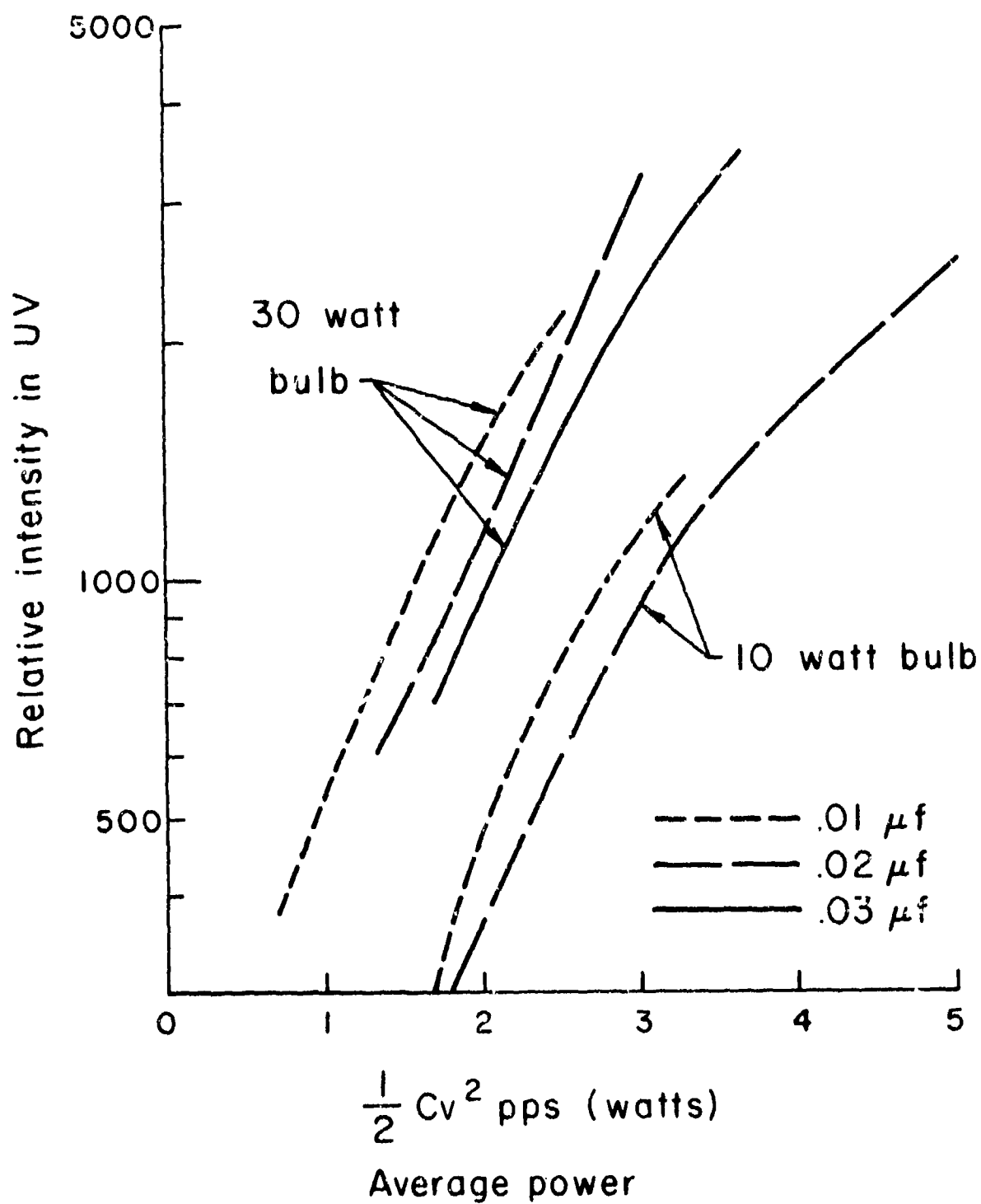


Figure 8. Relative energy conversion of USSI bulbs.

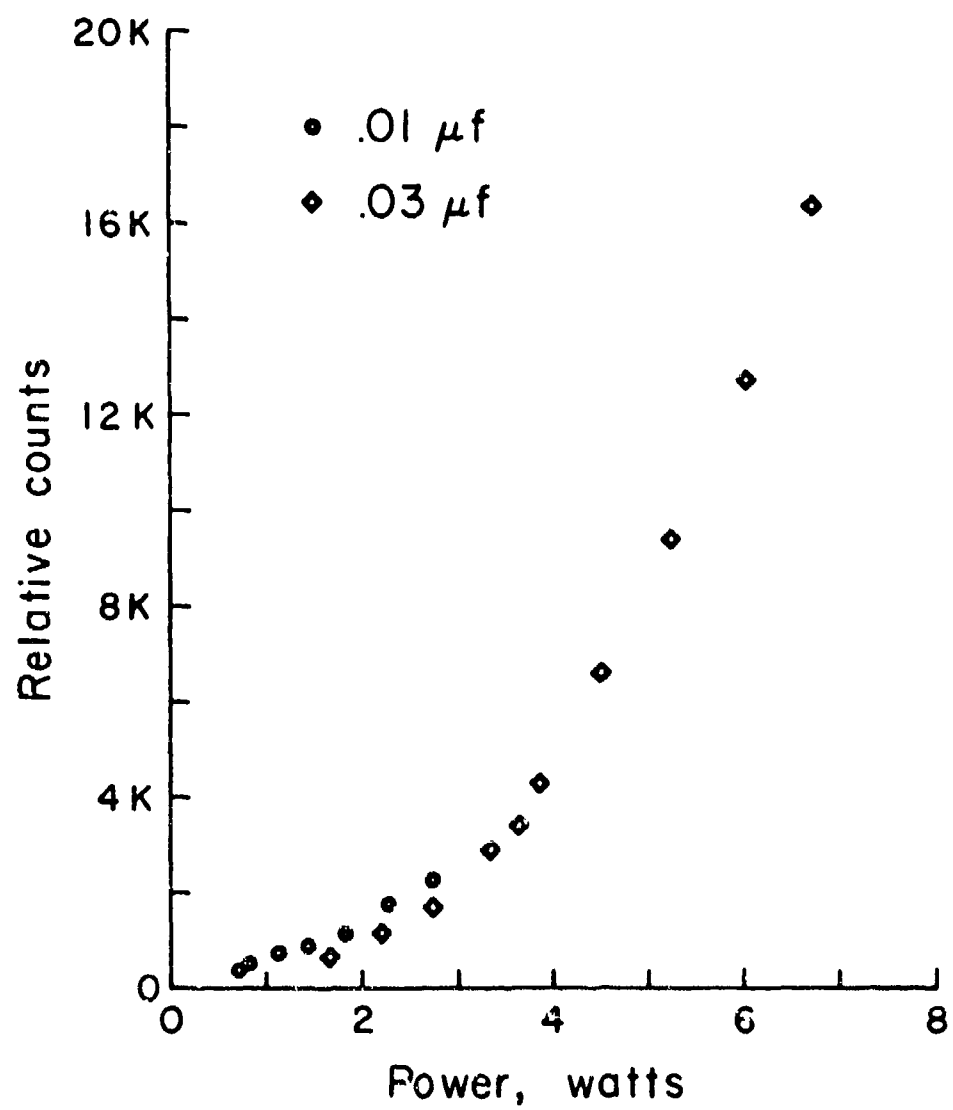


Figure 9. Power response of 30 watt USSI bulb.

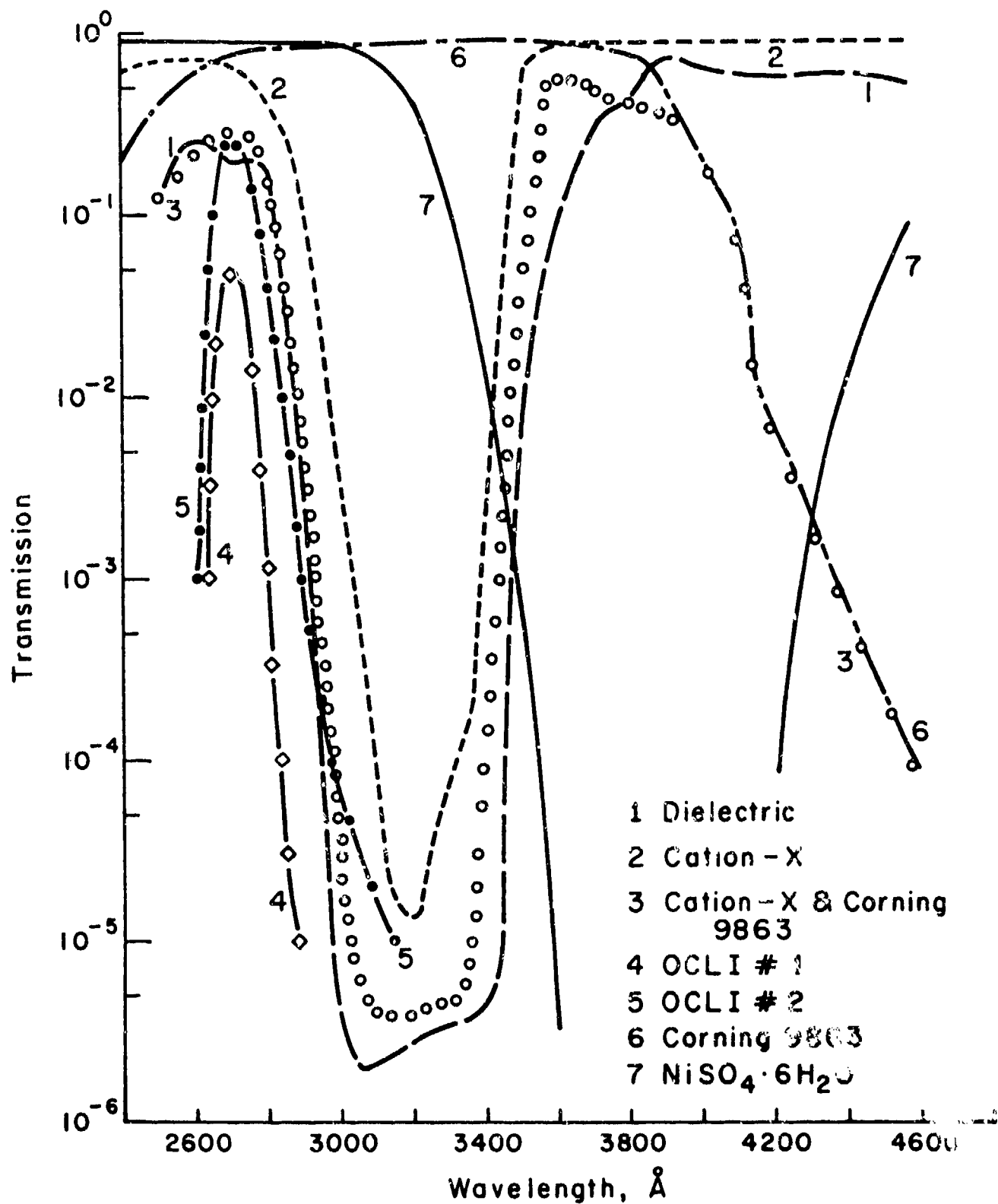


Figure 10. Transmittance curves of materials employed in solar blind systems.

provided by Barr Associates, Cambridge, Massachusetts. Filters have been developed by the author (Ref. 2), in collaboration with Optical Coating Laboratories, Inc. which were 0.25-inches thick but with a peak transmittance of 1.5% at 2630Å. Under the present contract, five filter combinations have been obtained from Barr Associates to provide considerable flexibility in selecting several wavelength intervals between 2200Å and 2800Å with considerable variations in long wavelength rejection. The transmission characteristics of these filters are indicated in Figures 11 and 12. Filters 1 and 2 are the basic filters necessary to obtain a high degree of solar blindness. The other three filters, used with the basic filters, provide wavelength discrimination in the spectral region between 2400Å and 2700Å. When these supplemental filters are combined with the PMT and the basic filters, we obtain the overall system spectral response shown in Figure 13. These elements are shown in Figure 14.

An additional 0.5-inch piece of $\text{NiSO}_4 \cdot 6(\text{H}_2\text{O})$ has been used in conjunction with the basic filters nos. 1 and 2 and the 2680 filter. The purpose of this additional filter is to eliminate the effects of a light leak at 4000Å associated with an "off design" photomultiplier tube described in the next section. Although the $\text{NiSO}_4 \cdot 6(\text{H}_2\text{O})$ filter has a transmittance of approximately 95%, the net effect including a reduction in field-of-view is a 21% decrease in signal. The field-of-view function (FOV) for this combination of filters has been determined experimentally by observing a point source of light at various angles from the detector optical axis. The results are shown in Figure 15 and have been included in the simplified scattering model described in a later section. The total field-of-view is seen to be approximately 28° with a half-angle (defined as the half-angle at 50% maximum intensity) of 7°.

For the purpose of measuring the atmospheric attenuation coefficient, it is necessary to point the detector directly at the source with a very narrow field-of-view. The purpose of the narrow field-of-view is to separate transmitted light from scattered light.

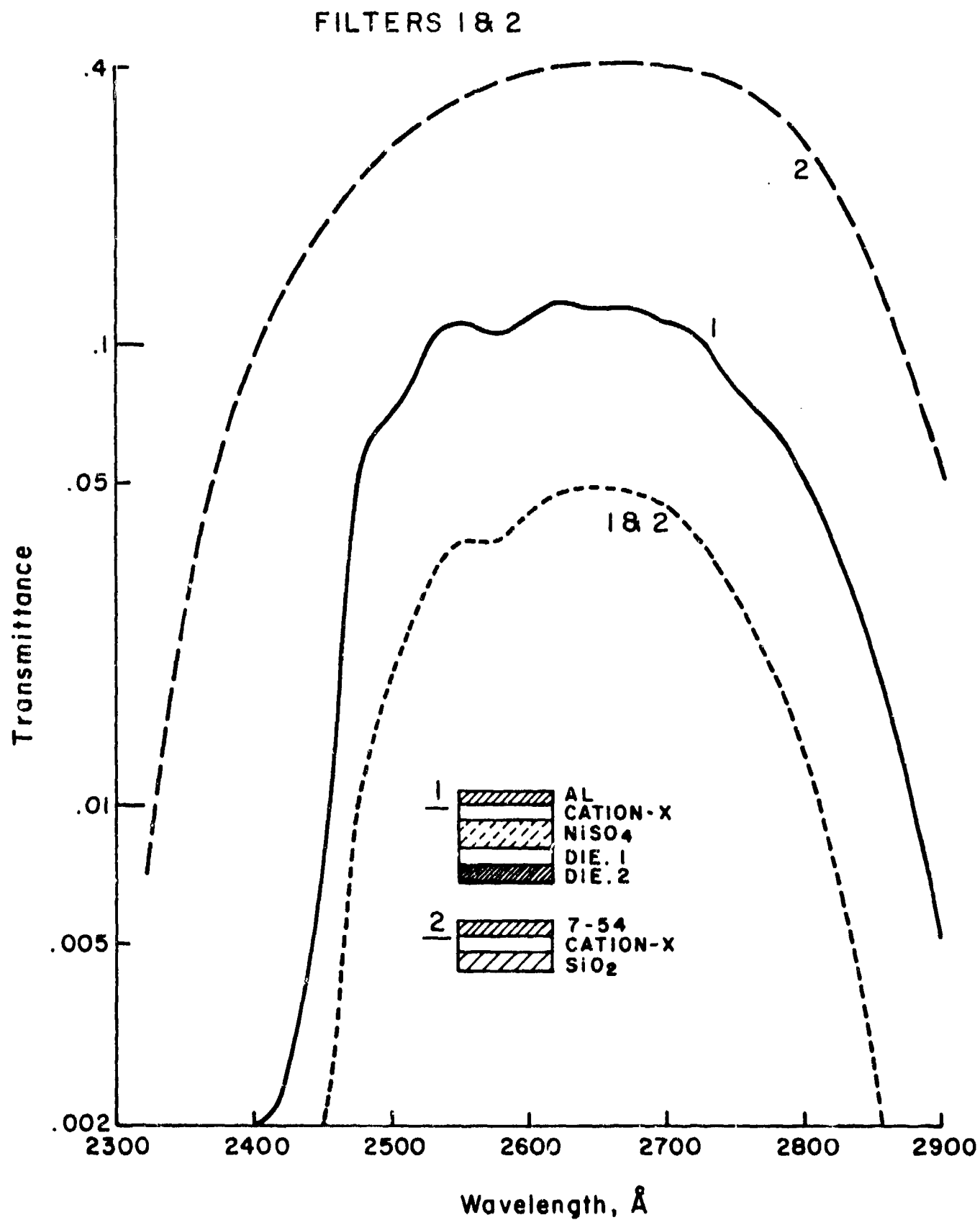


Figure 11. Transmission characteristics of basic filters 1 and 2.

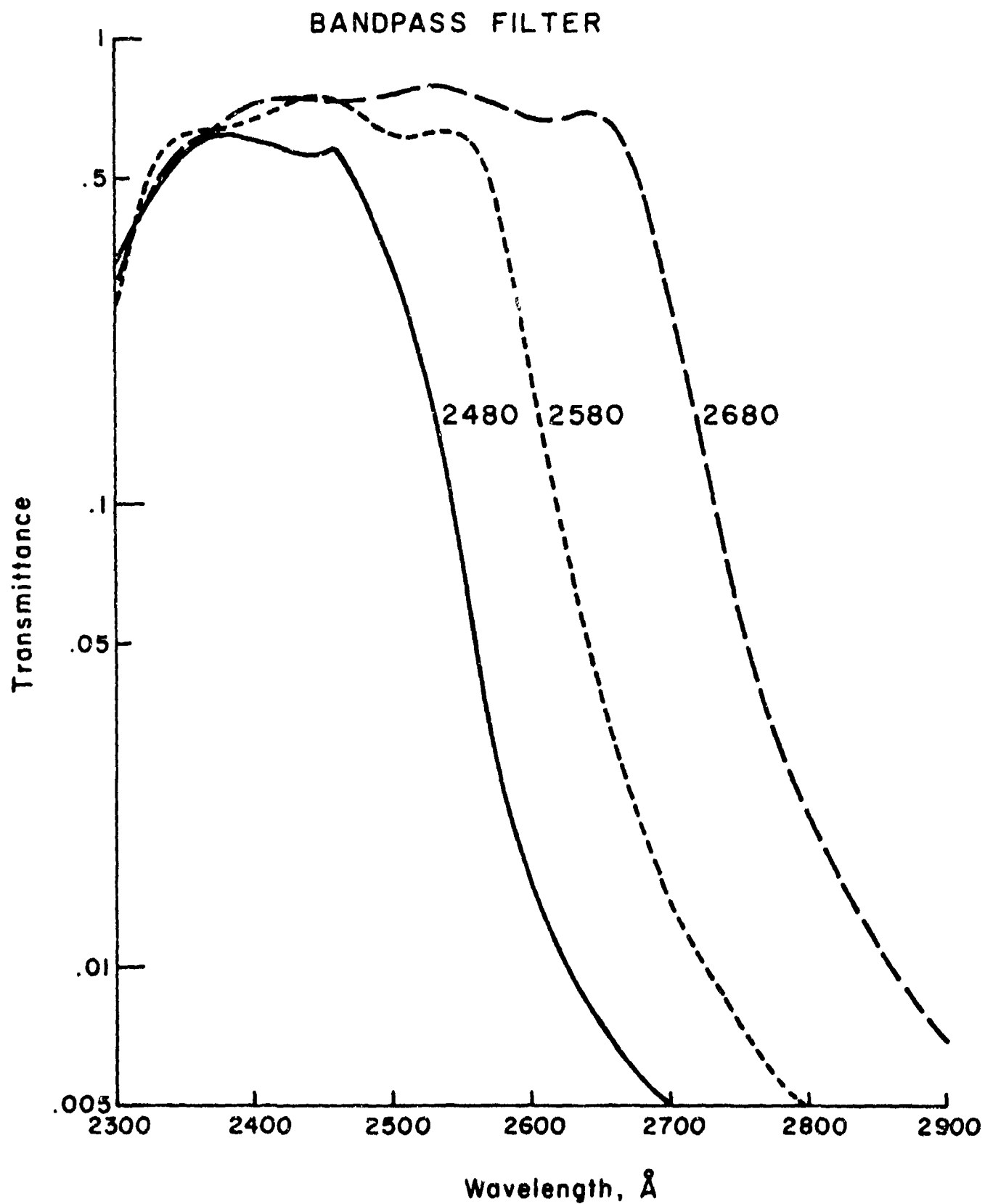


Figure 12. Transmission characteristics of 2680, 2580, and 2480 filters.

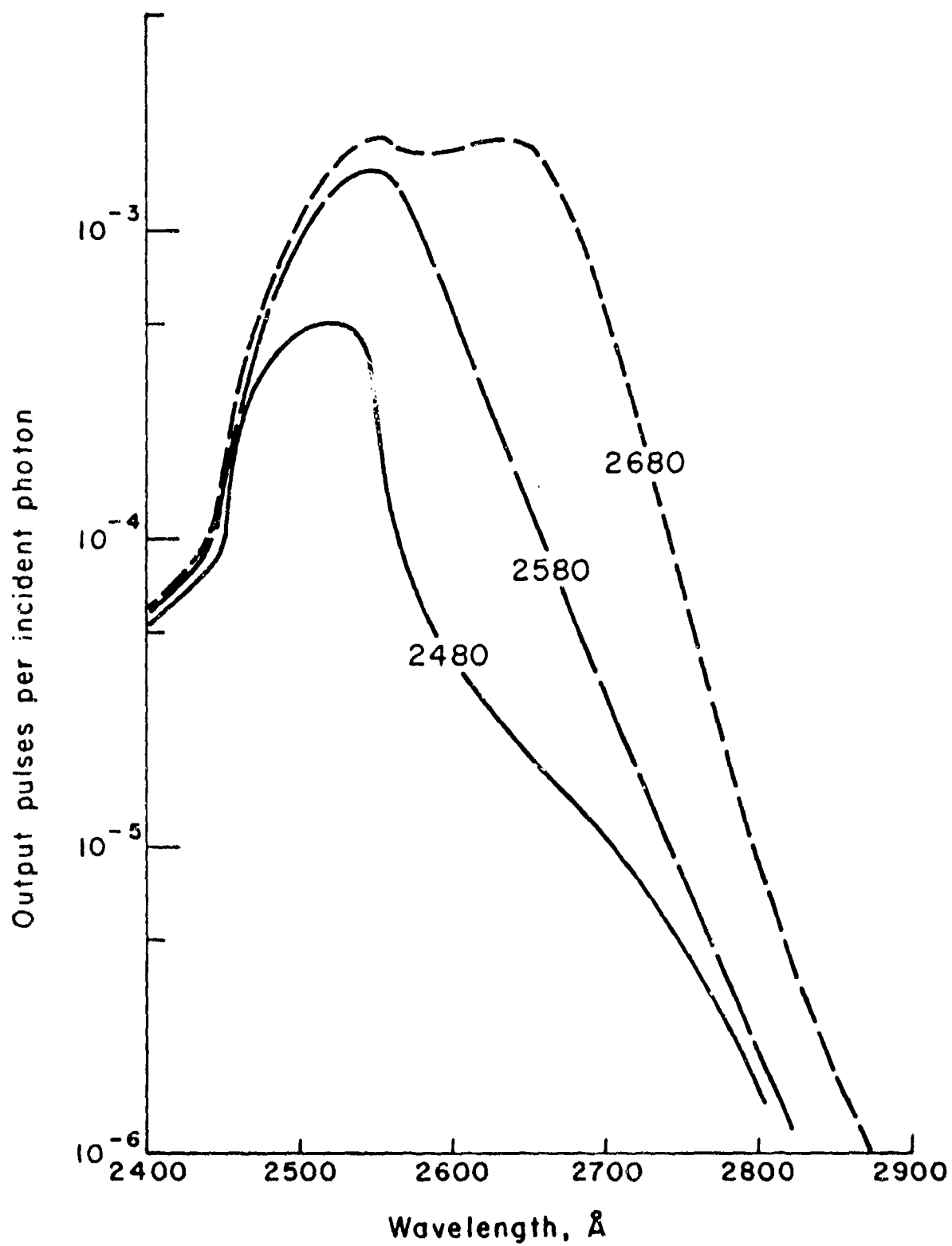


Figure 13. Overall system spectral response for the 2480, 2580, and 2680 filters.



Figure 14. Photograph of components of filter assembly.

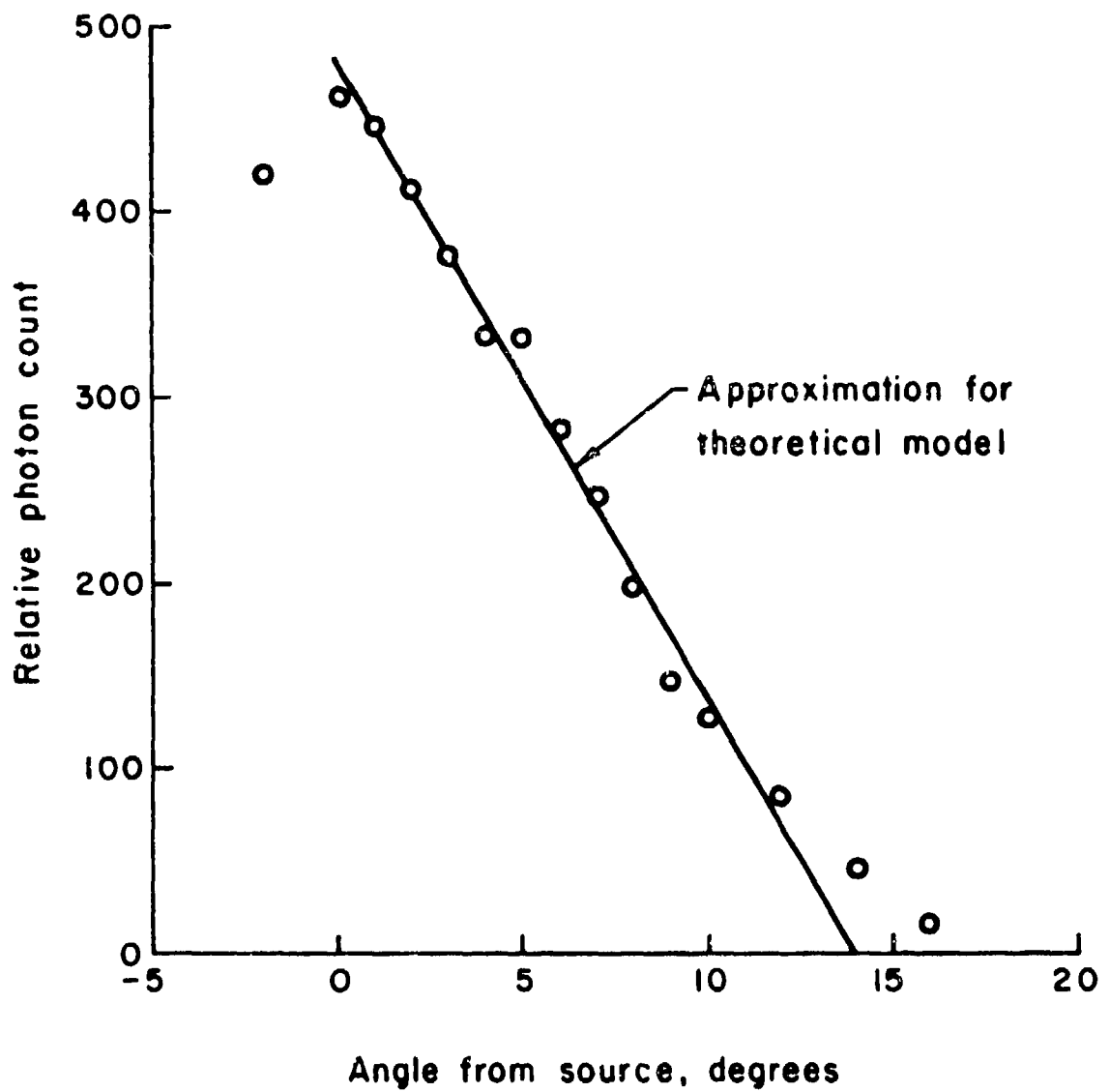


Figure 15. Angular dependence of field of view function.

A quartz lens with a four-inch focal length was therefore attached to the front of the filter assembly. Four inches behind the lens, a black aluminum disk with a 1/16-inch diameter hole was inserted. This combination of lens and stop yield a flat field of view function with a total angle of only 1.8°. For atmospheric scattering measurements, the stop and lens were removed.

Photomultiplier

The basic photomultiplier employed in this investigation was the 542P-09-18 provided by EMR. This tube has a rubidium telluride photosensitive cathode with the quantum efficiency as given in Figure 16. The particular advantage of this tube is the very low dark count (the random emission of electrons by the photosensitive cathode) which is approximately 10 counts/sec. A very low dark count is important in the measurement of atmospheric scattering since we can measure much lower levels of radiation. In addition, since this tube provides a very large dynamic range, 10^7 , very high levels of radiation can be measured.

Detection System

The basic electronic circuitry has been designed around the detection of the weakest signals from the ultraviolet source. The pulse of electrons produced at the anode of the photomultiplier, which is initiated by the ejection of an electron from the photosensitive cathode, typically has a pulse width of 40 nanoseconds (ns). This type of pulse is ideally suited for digital logic data processing.

The basic detection system is shown in Figure 17 which also indicates the various components. Figure 17a is a photograph of the detector and the HP counter employed for photon counting. The filter assembly also is shown. Figure 17b indicates the various components comprising the detector. The EMR photomultiplier (PMT) is a replacement for the original PMT which rapidly lost sensitivity

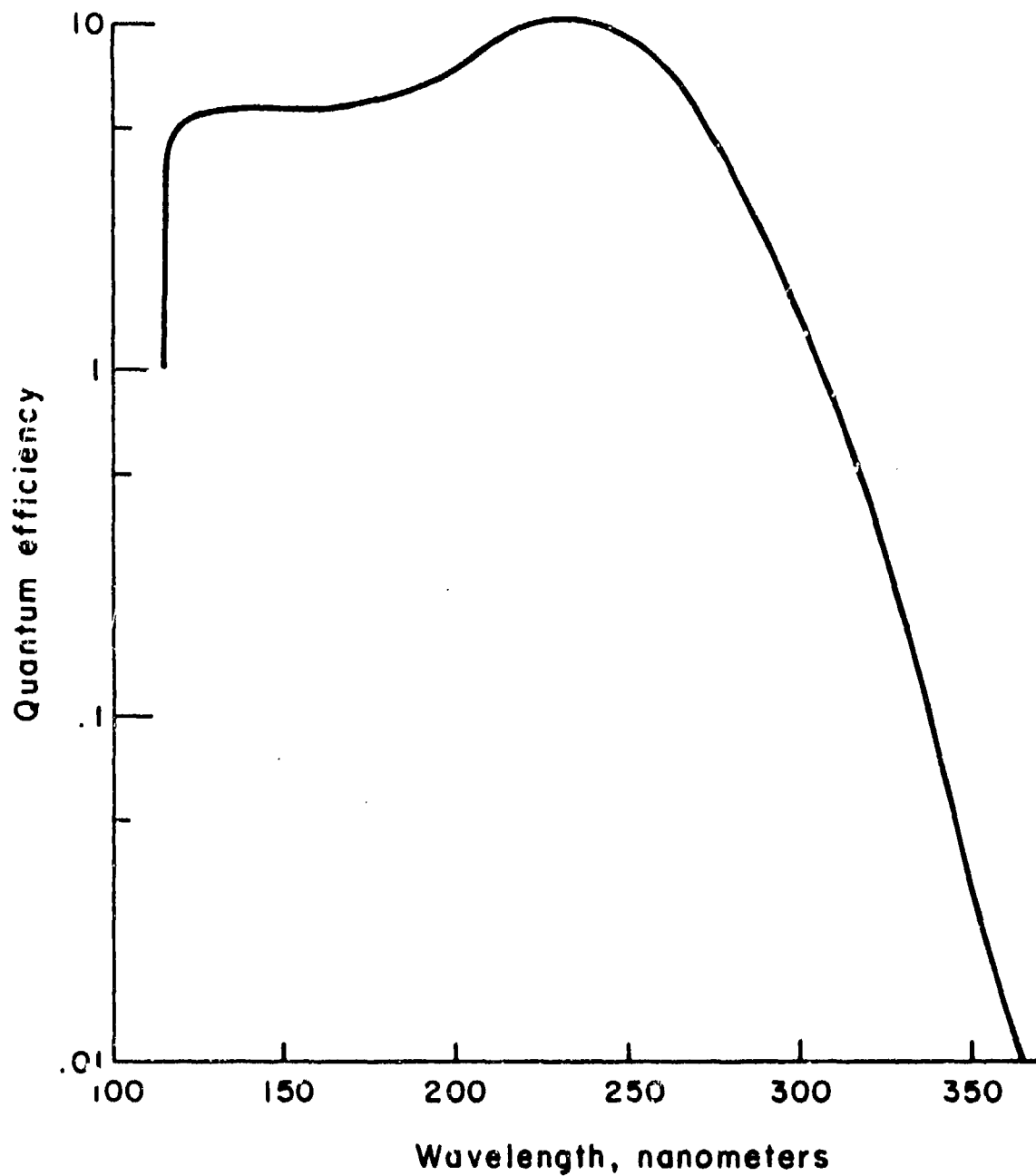


Figure 16. Measured quantum efficiency for EMR 542P-09-18 photomultiplier.

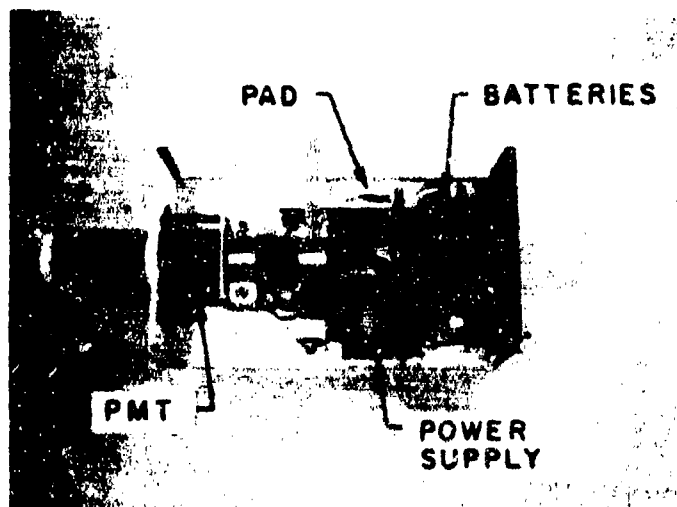
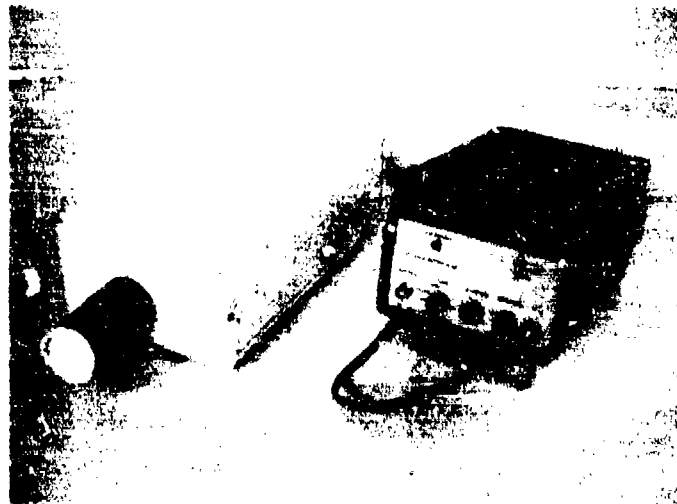


Figure 17. Photographs of the basic detecting system indicating pertinent components.

over a period of one day. The replacement PMT does not have the long wavelength rejection normally associated with EMR rubidium telluride PMT's. However, EMR did not plan to make any new tubes in the near future. Therefore, they searched their archives containing tubes which did not meet their very tight requirements. The present tube evidently did not meet their required long wavelength rejection. Although some radiation around 4000\AA can be detected, the amount is small and has not hindered our measurement effort. The EMR power supply, which converts 28V-DC to 2000-3600V-DC, also failed but was replaced by EMR.

The pulse amplitude discriminator, PAD, provides a very large range in sensitivity. This PAD amplifies the 40ns (nanoseconds) pulses from the PMT and produces a positive pulse of 60ns and 3.5 V-DC. The maximum random count rate is 4×10^6 cts/second.

Since the basic mode of measurement is that of pulse or photon counting, all measurements indicate the number of photons/sec detected by the system. This type of measurement permits a wide dynamic range. All measurements are in terms of cts/sec or cts/time interval. The dark count of the system is the number of counts received per second with the entrance aperture completely closed. The count can be varied somewhat by the sensitivity level set by the PAD. Under normal conditions the dark count ranges between 6 and 15 cts/sec.

The apparatus which was used to obtain field measurements of scattered radiation is shown in Figure 18. The table mounted on a tripod contains the detection system, a telescope for sighting on the source, a compass used to obtain bearing and azimuthal angle from source, and a device to measure elevation angle.

Transmitter and Receiver

Voice communication has been achieved employing a breadboard

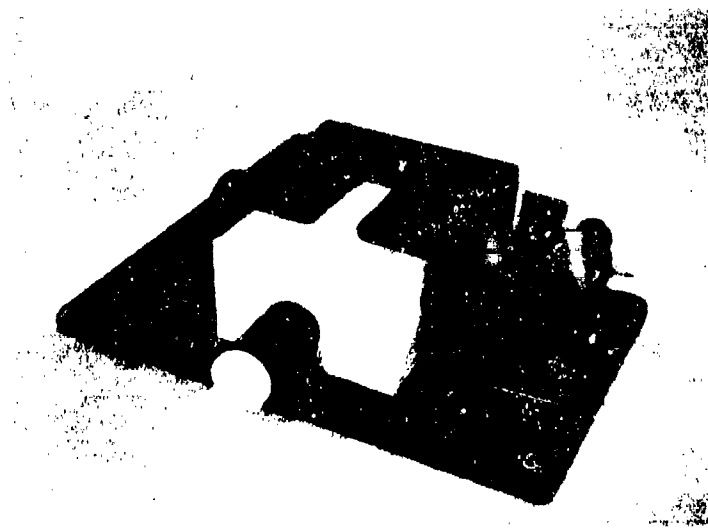


Figure 18. Apparatus employed to obtain field measurements of scattered radiation.

transmitter and receiver. The system employs pulse frequency modulation with a center frequency of 4810 pps. The voice bandwidth is restricted to the interval 200 Hz - 2000 Hz. Figures 19 and 20 indicate block diagrams of the associated electronic circuits.

This particular system includes a feature which helps to eliminate random pulses. This is achieved by a minimum interval detector. After receiving a pulse the system will not admit another pulse of 167 μ sec. Then the system is "on" for 83 μ sec to admit the next pulse. In this manner, extraneous pulses tend to be eliminated.

At the present time, the transmitter circuit does not have all of the elements indicated in Figure 19. The automatic gain control, AGC, and the logarithmic speech compressor have not been installed. The receiver circuit has all of the indicated elements.

Our basic detection system, including the EMR-PMT, was used as the front end of the receiver. The 60 ns output pulses were too sharp for the input buffer circuit. Therefore, a fast one-shot multivibrator was used to stretch the pulse to 6 μ sec.

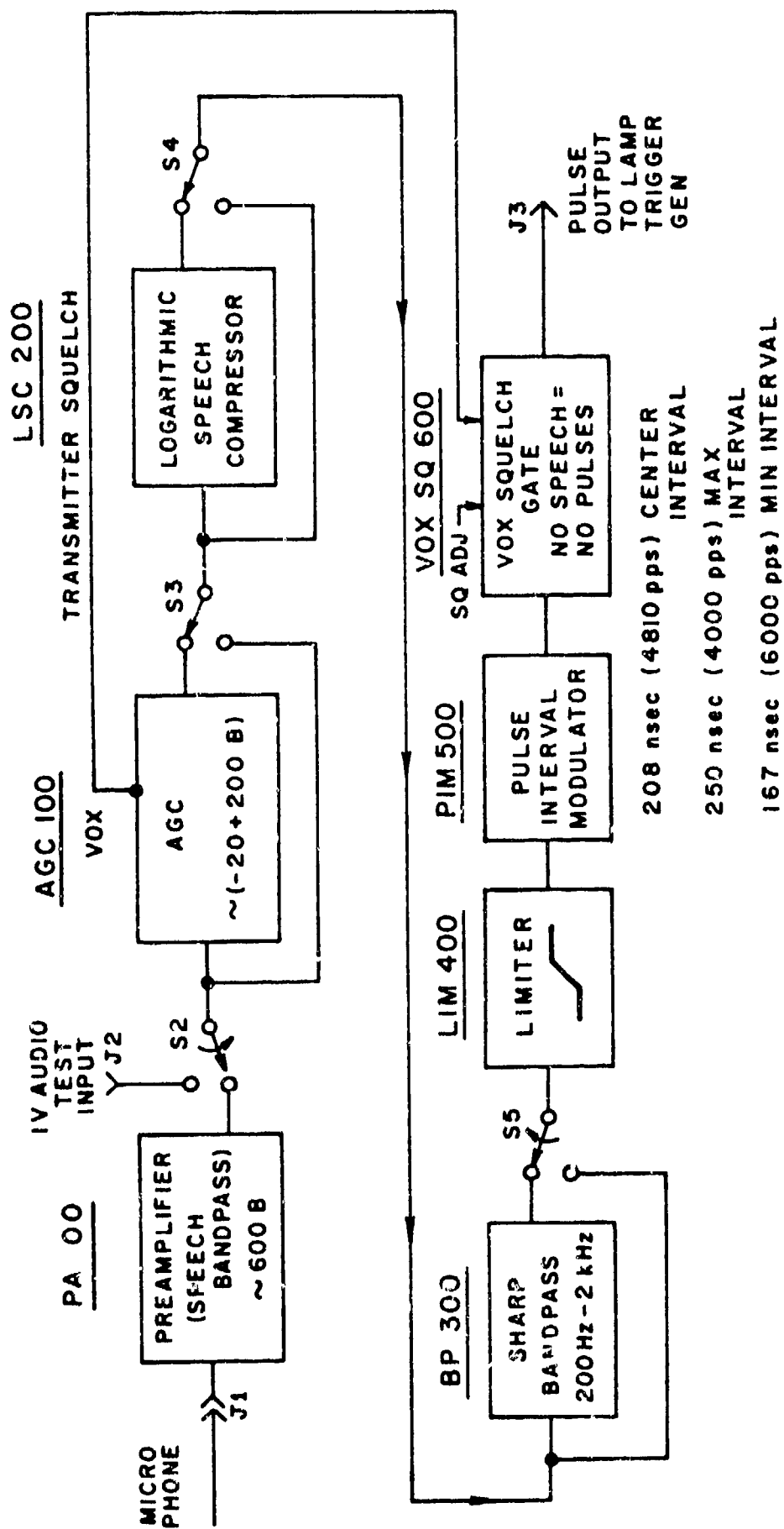


Figure 19. Signal processing - transmitter.

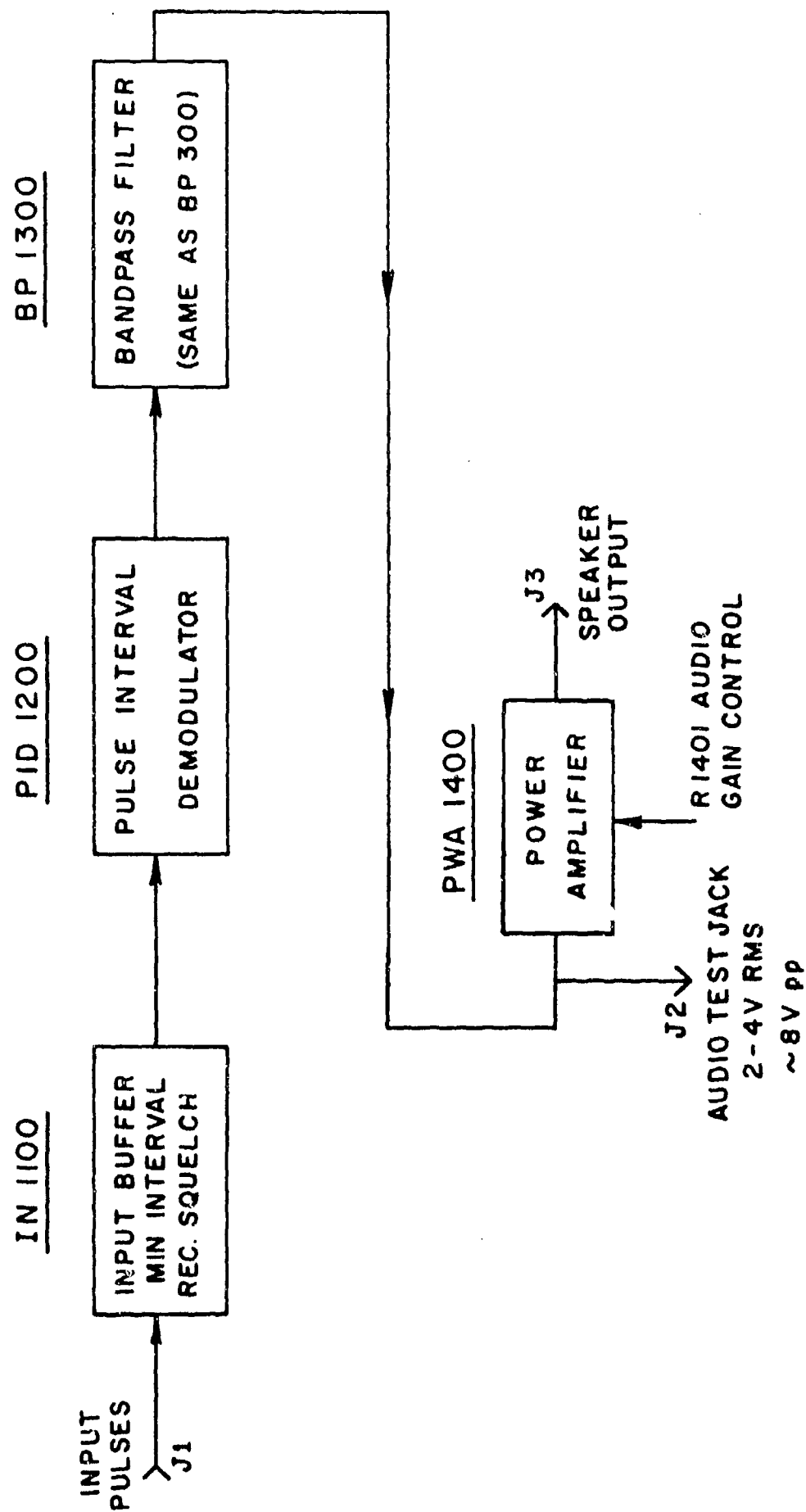


Figure 20. Signal processing - receiver.

III. MEASUREMENTS

The purpose of the field measurements was to evaluate the potential of nonlinear sight communication via scattered ultraviolet radiation in the lower atmosphere. A primary concern in the evaluation of the communication system is the possible interference which might arise due to natural and manmade UV sources. Thus, the first phase was the determination of the ambient background. The next step was the determination of the manner in which the atmosphere processes a flash of UV photons. The magnitude of UV scattering and absorption by the atmosphere was determined by surveying the sky from various locations away from the source. In addition, to correlate the data with our mathematical modeling, it was necessary to determine experimentally what portion of the received signal came from the lower part of the field of view and what portion came from the upper part. Finally, field measurements provided first-hand experience in determining problems which might arise with an actual UV communications system.

Background Measurements

The most significant background measurements were those obtained during relatively clear, sunny days in which solar radiation was expected to be the dominant source of scattered UV radiation. Numerous measurements were made employing various filter combinations. These measurements included those in which the sun was directly in the detector field of view. The results are indicated in Table 1. This table contains two sets of measurements approximately one hour apart. The bearing and elevation of the sun corresponded to the beginning of the first set of measurements. Because of the long wavelength "leak" around 4000\AA , we used a long wavelength filter, LWF, which was opaque to radiation below approximately 3700\AA . To determine the UV radiation detected by the system, we would make

TABLE 1
TYPICAL RESULTS FROM SKY SURVEY
SUN AT BEARING 255° ELEVATION 48°
SYSTEM DARK COUNT 5.2 CTS/SEC OVER 50 SECONDS

FILTER COMBINATION	BEARING	ELEVATION	AVERAGE CTS/SEC	TIME PERIOD SEC	UV CTS/SEC
1,2	45	20	44.7	50	31.3
1,2,LWF *	45	20	13.4	30	
1,2	90	20	41.0	40	25.3
1,2,LWF	90	20	15.7	30	
1,2	225	20	55.1	30	32.9
1,2,LWF	225	20	22.2	30	
1,2	315	20	63.9	30	44.0
1,2,LWF	315	20	19.9	20	
1,2	270	20	76.1	40	47.3
1,2,LWF	270	20	28.8	20	
1,2,2680	270	20	14.3	30	0
1,2,2680,LWF	270	20	14.5	30	
1,2	DIRECTLY AT SUN		52.3	70	21.1
1,2,LWF	"	" "	31.2	50	
1,2,2680	"	" "	14.5	60	0
1,2,2580	"	" "	16.8	90	0
1,2,2480	"	" "	17.2	40	0
1,2,2480,LWF	"	" "	15.7	60	0

*LWF is a filter transparent at wavelengths longer than 3700Å.

one set of measurements without the LWF and one set with the LWF. Thus, the detected UV radiation would be the difference between the two measurements. This value is in the last column. Filters 1 and 2 do permit some solar radiation in the 2800-2900Å spectral region to reach the PMT. This problem was anticipated and, in fact, the filters were designed in that manner. However, when any of the 2680Å, 2580Å, and 2480Å filters were used with 1 and 2, no solar UV radiation was detected. The counts received when these filters were employed corresponded to the "leak" around 4000Å. The last series of measurements with 1, 2, and 2480 with and without the LWF clearly indicates that no solar UV radiation is being detected. The count level of approximately 14-17 is composed of 5.2 counts of average dark count and the remainder from the leak at 4000Å. In all measurements after this initial set, one of the three filters 2680Å, 2580Å, and 2480Å was always employed with 1 and 2.

The basic filter combination of 1, 2, and 2680Å was extensively employed in measurements of the natural and manmade backgrounds in and around Princeton and Trenton, N.J. Considerable time was devoted to this task. Surveys were made during daylight hours and early evening hours. The early evening hours included times during which street lights and neon signs were on. The count rate never at any time indicated a source of UV radiation in the spectral region below 2800Å. Counts were registered due to noisy transformers in the neonlights but no UV radiation was detected. This result was not surprising since all manmade sources of illumination have glass covers which do not radiate below 2800Å.

Measurements have been made of possible UV radiation emitted by lightning during thunderstorms. A number of lightning strokes were observed with ranges from 0.6 km to 4 km. Low counts were observed, in the 400-600 count region, but these were most probably due to the electrical disturbance produced by the lightning. Similar counts were recorded with the aperture open and closed. Thus, the UV radiation which may be produced by lightning strokes is negligible.

As expected, the ultraviolet radiation emitted from flames was detectable with the UV system. The flames from matches, lighters and propane torches were used on several occasions to test the vulnerability of the UV communication system to background noise. Unfortunately, no opportunity arose during the course of the measurements to observe a large fire such as a burning building. Nor did an opportunity arise to measure the effects of explosives and munitions.

High Energy Flashlamp Measurements

Two basic types of measurements were made using the high energy flashlamp. By pointing the detector directly at the source from various distances, the line-of-sight attenuation coefficient was measured. The attenuation coefficient is a direct measure of the number density and cross-sections of atmospheric absorbers and scatterers on a given day. Alternately, the detector was pointed away from the UV source, so as to systematically determine the amount of scattered radiation coming from various portions of the sky. These maps, which indicate the way in which UV radiation is processed by the atmosphere, are referred to as scattering "footprints."

Attenuation Measurements

In principle, the measurement of attenuation coefficients is straightforward. The attenuation coefficient $\sigma_A(\lambda)$ is defined

as the fraction of light removed or deflected from its original direction due to absorption and scattering, per unit path length at wavelength λ . In the case of radiation passing through a uniform atmosphere from an isotropic source, the relation between the transmitted and initial intensity is

$$I(R) = \frac{I_0 e^{-\sigma_A(\lambda)R}}{4\pi R^2} \quad (1)$$

where the initial source intensity I_0 is in units of photons per flash, $I(R)$ is in units of photons/km²/flash, and σ_A is in units of 1/km. If σ_A is equal to zero, then the above relation reduces to the simple inverse square law. If the area of the detector entrance optics is A_D and the conversion efficiency of captured photons to photon counts is FOV (the field-of-view function), then the photon count PC due to a single flash of photons at wavelength (λ) is

$$PC(\lambda, R) = \frac{(FOV)A_D I_0}{4\pi R^2} e^{-\sigma_A(\lambda) \cdot R} \quad (2)$$

Because an accurate value for the combined term $(FOV)A_D I_0$ is not always known, the value of $\sigma_A(\lambda)$ is usually obtained by measuring $PC(\lambda)$ at two different distances R_1 and R_2 . The attenuation coefficient can then be solved from the relation

$$\sigma_A(\lambda) = \frac{1}{R_2 - R_1} \ln \frac{R_1^2}{R_2^2} \frac{PC(R_1, \lambda)}{PC(R_2, \lambda)} \quad (3)$$

In the present study, measurements have not been made at discrete wavelengths but rather over narrow bands such as those shown in

Figure 13. Therefore, it has been assumed that the attenuation coefficients measured using the above equation are average values over the width of the band.

The attenuation coefficient actually represents both the decrease in total UV radiation due to ozone absorption and the deflection of UV radiation due to scattering. The basic difference between absorption and scattering is that with scattering the photons are not removed from the atmosphere but merely change direction. The attenuation coefficient σ_A can be written as the sum of the absorption coefficient and the scattering coefficient.

$$\sigma_A = \sigma_{ABS} + \sigma_{SCATT} \quad (4)$$

It is important to the successful measurement of the attenuation coefficient that scattered light be prevented from entering the detector when the light source is viewed head on. For this reason, a very narrow detector field of view is required, because scattered light will reach the detector from all angles while transmitted light comes virtually from a "single" angle (see Figure 21). While it is not possible to completely eliminate scattered light, it is possible to reduce it to a level where it will be small compared to the transmitted light.

Actual values of the attenuation coefficient as measured in the field varied from 1.6/km to 3.2/km which is consistent with the values reported by Baum and Dunkleman (Ref. 3) as shown in Figure 22. Early in the study, however, the values of the attenuation coefficients obtained between the various sites on a given day were not consistent. An investigation into the origins of the inconsistency showed that errors in the attenuation coefficient could result from the following:

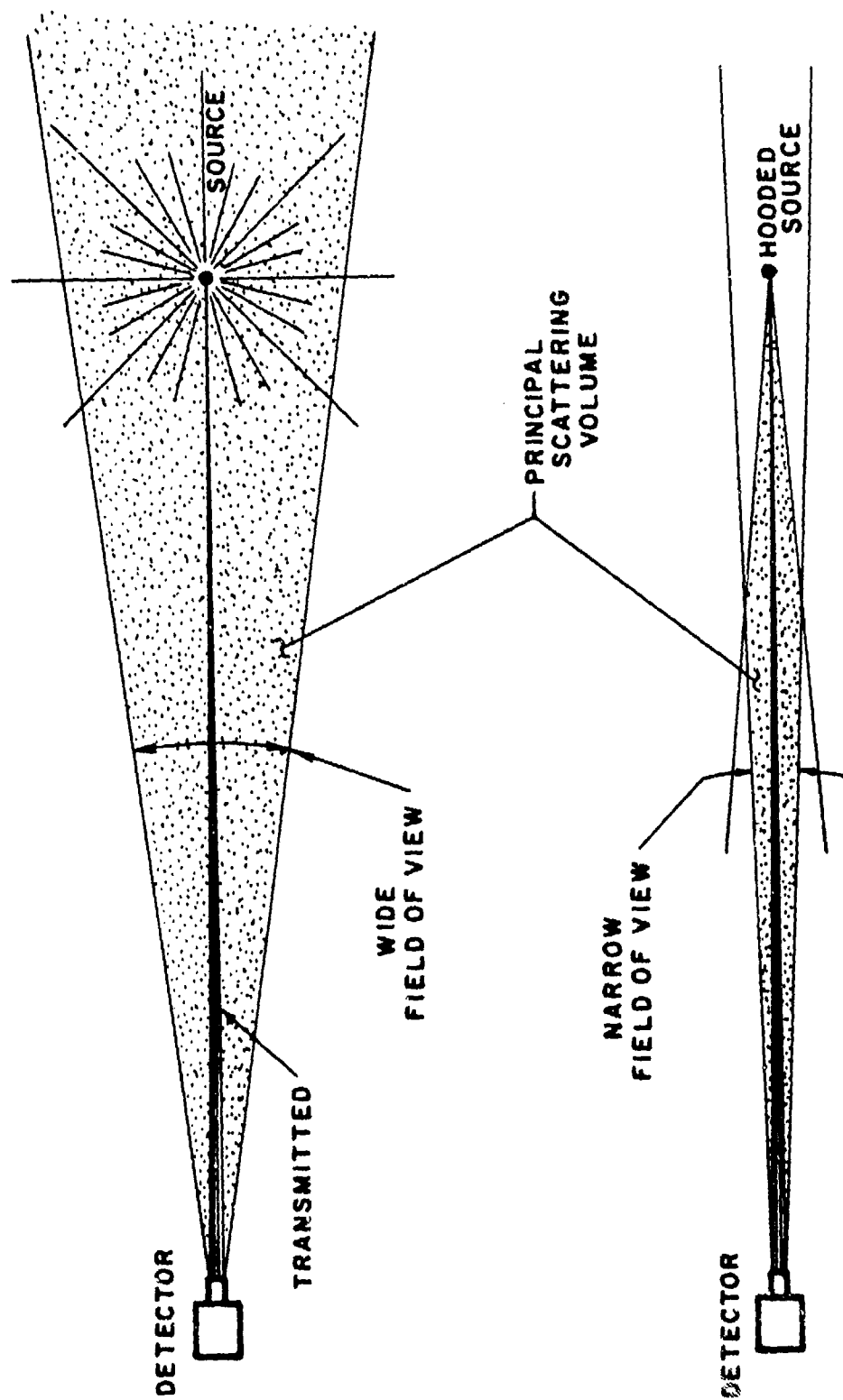


Figure 21. Reduction of scattered light for measurement of attenuation coefficient.

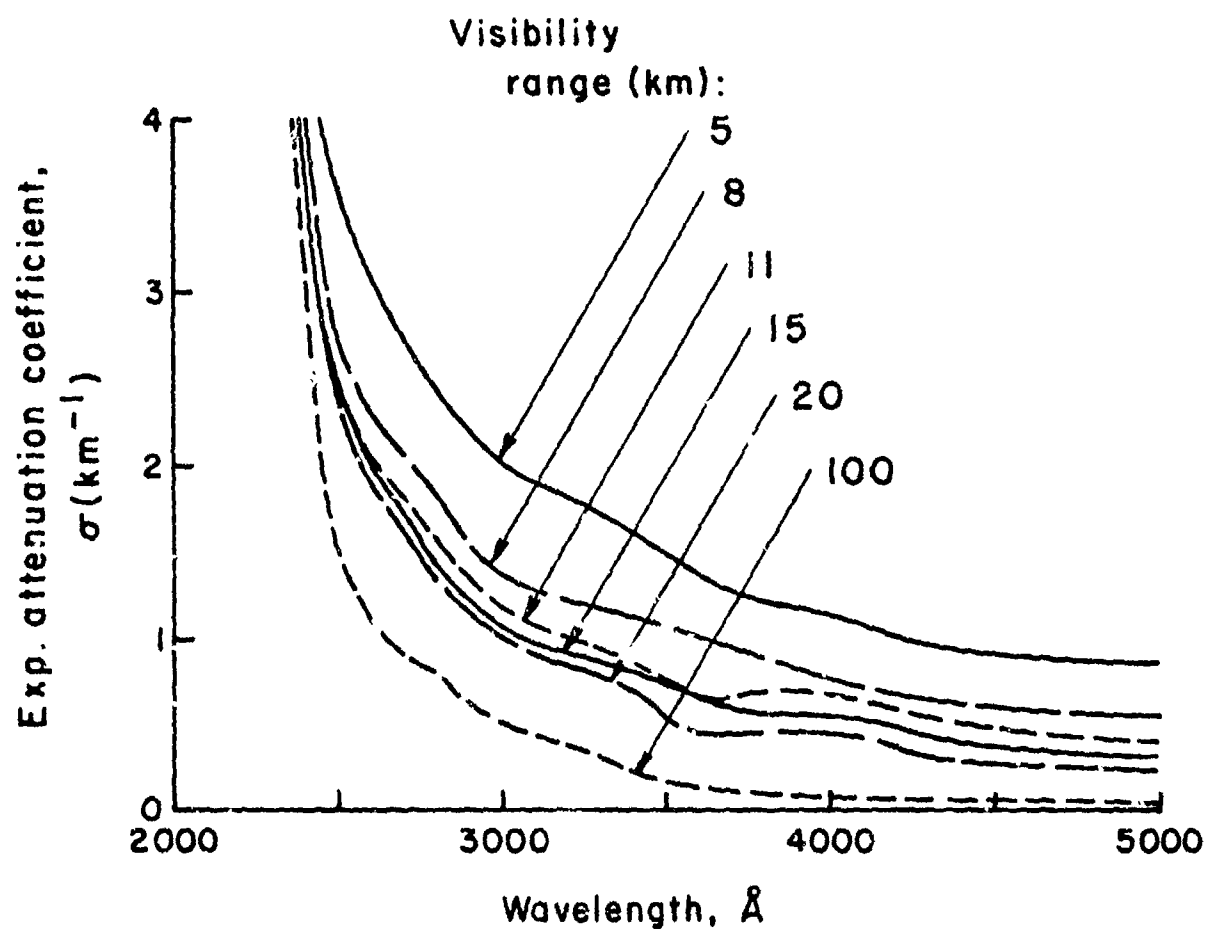


Figure 22. Baum and Dunkelman attenuation data.

incorrect distance measurements

changing visibility during the course of the measurements

imprecise pointing of the detector toward the source

interference from scattered radiation

changing flashlamp intensities

scintillation error

change of attenuation coefficient with distance

The results of the analysis showed that while interference from scattered radiation can result in the measured attenuation coefficient being lower than the actual value, the low values should be consistent with each other. Although the measured coefficients can be very sensitive to errors in the distance measurements and errors in the pointing of the detector, sufficient care was taken in obtaining the measurements so as to avoid these particular problems. The measurements were found to be very repeatable so as to rule out changing flashlamp intensities and scintillation errors. Although the attenuation coefficient may decrease with distance due to preferential attenuation of the lower wavelength light within the band, or due to spatial nonuniformities of the atmosphere, the observed inconsistencies were opposite to those expected from these effects. The major contributor to the inconsistencies was found to be the changing visibility during the time the measurements were obtained.

Several steps were taken to remedy this problem. Measurements were subsequently made in the afternoon as opposed to before noon, when the early morning haze was still being "burned off." The detector pointing process was greatly simplified to save time.

A hood was placed over the lamp to eliminate scattered radiation in all but the immediate forward direction (see Figure 21). Attenuation measurements were completed as quickly as possible before any scattering measurements were begun. In this manner, completely consistent measurements were made between various sites.

Experiments have been carried out to simultaneously measure the attenuation coefficient at three different wavelengths using the filters described in Figure 13. The attenuation coefficients measured using the 2680, 2580, and 2480 filter combinations were 2.65, 3.05, and 3.05 respectively. Visibility was observed to be between 5 and 10 km, which is consistent with the data shown in Figure 22. It is worth noting in Figure 13 that the three filters, when used in combination with filters no. 1 and 2, do not peak at the same wavelength as they do in Figure 12.

Scattering Measurements

The procedure for mapping atmospheric scattering footprints is shown schematically in Figure 23. The source was located at some slightly elevated position, such as the roof of a relatively low building, and the detector was moved some distance x away. In all cases, the detector-to-source line of sight was within 3.5 degrees of the horizontal and was defined as zero azimuth and zero elevation. Typically, the detector optical axis was raised vertically to some angle of elevation denoted as ELEV and then rotated in the horizontal plane to some azimuthal position denoted as AZIM. The flashlamp was flashed from 3 to 5 times and the resulting detector photon counts were recorded. The procedure was repeated with the detector optical axis systematically rotated to various azimuthal angles and raised to various elevations.

For each position of the detector, optical axis background was measured by observing the photon count level between flashes of the

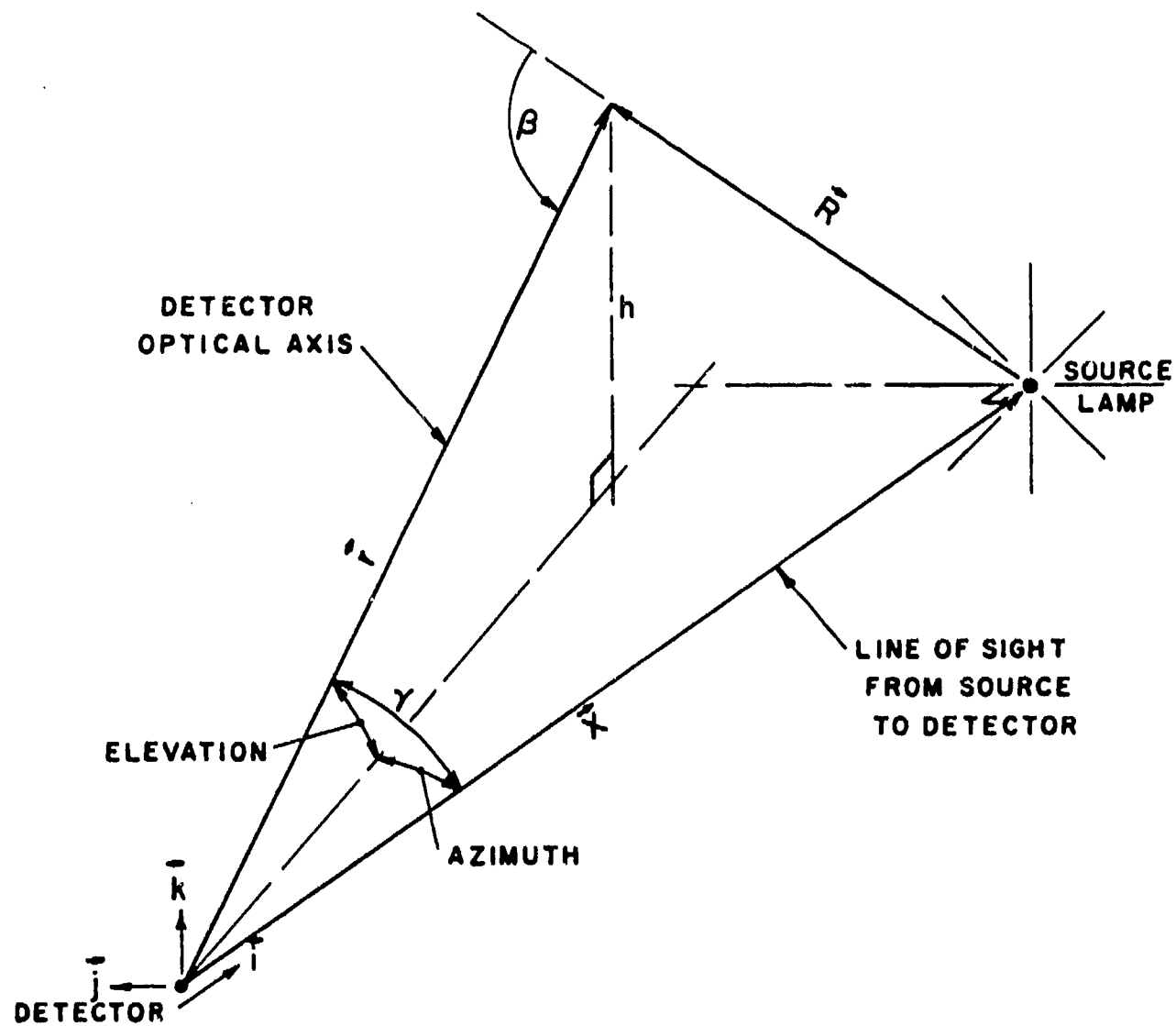


Figure 23. Geometry of atmospheric scattering measurements.

lamp. The data were later reduced by subtracting the averaged background count from the average flashlamp count at each position. On some occasions, the detector was moved to a second location and the entire procedure was repeated.

The very first series of measurements showed that the atmospheric scattering footprints were symmetric with respect to positive and negative azimuthal angles. In other words, the averaged reduced photon count at (20° ELEV, 45° AZIM) was equal to the count at (20° ELEV, -45° AZIM) and so forth. Subsequent measurements were therefore limited to azimuthal angles between either 0 and 180° or 0 and -180° but not both.

Samples of atmospheric scattering data obtained on two separate occasions at a distance $x = .82$ km are shown in Figure 24. Data were not obtained for zero elevation because of nearby bushes, trees, and other natural or manmade obstacles. The difference in magnitude of the photon counts on the two days was due in part to a change in the setting of the pulse amplitude discriminator, and in part to different weather conditions. If the data of Figure 24 are plotted as a function of the absolute angle γ , between the detector optical axis and the detector to source line of sight, we obtain the results shown in Figure 25.

The symmetry with respect to γ shown in Figure 25 was somewhat surprising when first observed. Prior to these experiments, it was expected that the intensity of scattered light would fall off at lower elevations due to absorption effects by the ground. It was later found that, due to strong preferential scattering in the forward direction, most of the photons reaching a given scattering volume are traveling very nearly in a radial direction from the source. This simple observation was easily confirmed by the high photon counts observed at the lower angles in Figure 25. Due to the symmetry with respect to the absolute angle γ , many

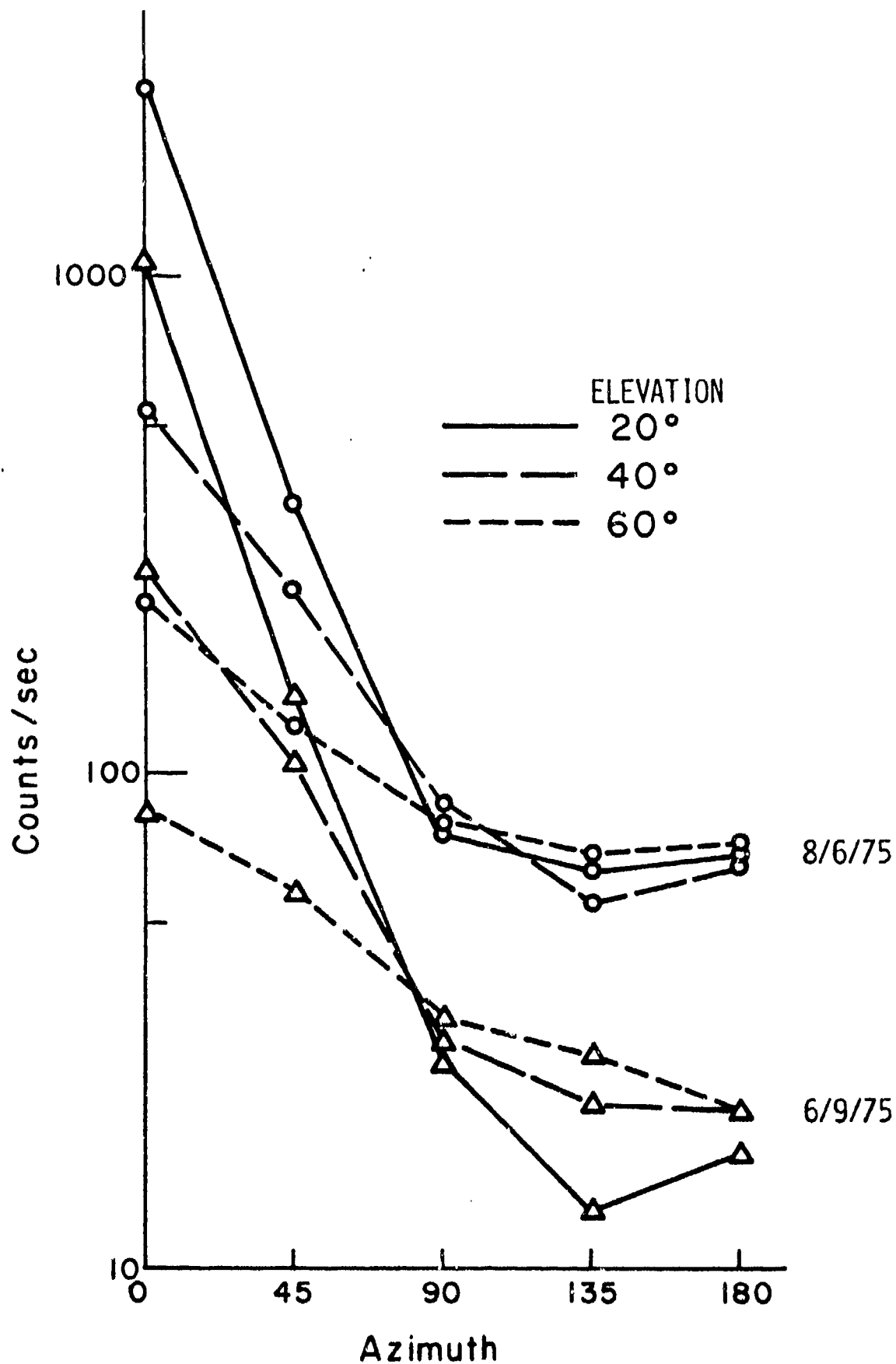


Figure 24. Atmospheric scattering footprints at .82 km.

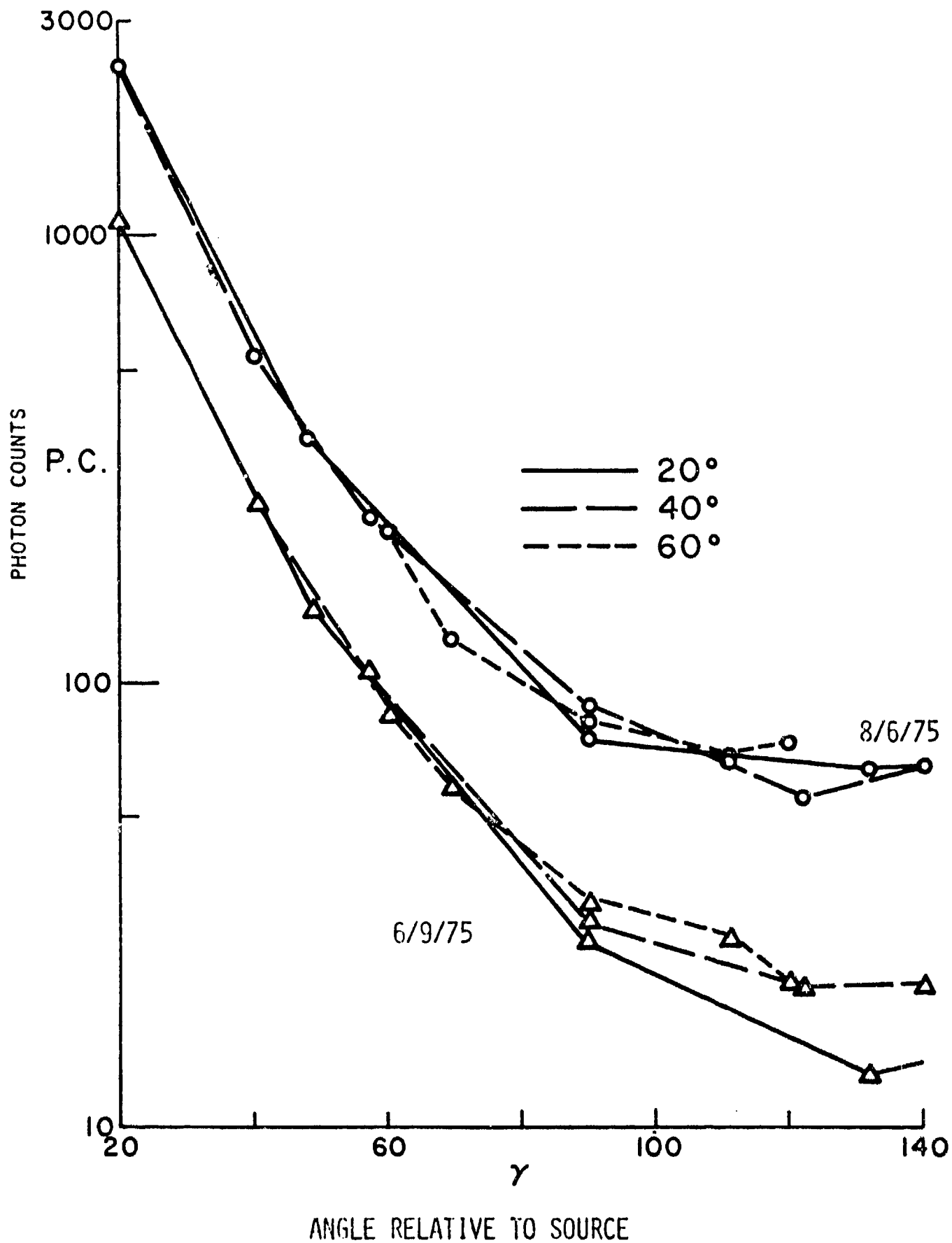


Figure 25. Symmetry of scattering footprints with γ .

experiments were restricted to an azimuthal angle of zero with elevations ranging from 0 to 160°.

Attempts were made on several occasions to obtain data at more than one source to detector distance x . Unfortunately, much of this data had to be discarded due to the inconsistencies in the measured attenuation coefficients as reported in the last section. Since the primary source of the inconsistencies was identified as changing atmospheric conditions, no meaningful conclusions could be drawn from the associated scattering data. In an attempt to minimize the possibility of changing atmospheric conditions, subsequent experiments were scheduled in the afternoons to avoid the burning off periods of early morning hazes and fogs.

The first two attempts to obtain scattering data in the afternoon at two different x locations were ruined by sudden large increases in the detector dark count. The source of the high dark counts was found to be the heat of the afternoon sun. The black lens holders (Figure 14) which held the solar blind filters were becoming hot to the touch and this heat was being transferred to the photomultiplier tube. Once the lens holders were painted white and a small sun shade was installed over the detector box, this type of increase in background count was no longer observed.

Finally, a procedure for obtaining scattering measurements and the associated attenuation coefficient was devised which gave consistent results. First, scattering measurements were made at the furthest location (2.08 km), and then a source-to-detector line of sight reading was obtained using the stop and lens as described in the apparatus section. The detector equipment was then quickly moved to the nearest location (.82 km) and another line of sight measurement obtained. Finally, scattering measurements were obtained at the nearest location. The entire procedure, from the first measurement at the furthest location to the last measurement

at the nearest location, required approximately 40 minutes. The results of one such measurement are shown in Figure 26. The associated attenuation coefficient was found to be 2.65/km. At the 2.08 km location, data were obtained at more than one azimuthal angle in order to check the symmetry already observed at the .82 km location. The symmetry appeared to be maintained, although the photon count for angles greater than 60° was less than 10 counts and therefore subject to scintillation error from the background count, which was of the order of 10-12 counts/sec. The dashed and solid lines on Figure 26 represent numerical solutions to a simplified atmospheric scattering model which will be presented in the next section.

Aluminum Reflector Experiment

An experiment was carried out to determine the effects of placing a small aluminum reflector under the flashlamps. Intuitively, it was believed that this reflector would increase the observed photon count by increasing the amount of UV radiation entering the atmosphere. At close range ($x = .2$ km), the photon counts were observed to increase significantly. The data obtained at $x = .82$ km, with and without the aluminum reflector, are shown in Figure 27. As can be seen, the photon count remained approximately the same, whether the reflector was used or not. These unexpected results were verified by repeating the experiment several times during a very short period of time. It was later observed, from a series of experiments discussed below, that there is a strong favoring of scattering in the forward direction. Consequently, very little of the radiation leaving the flashlamp in the vertical direction (the direction of light reflected by the plate) will later reach a point in the horizontal plane of the lamp. Conversely, the scattered light reaching the deflector can be significantly increased by rotating the aluminum reflector into the vertical plane behind the flashlamp, thereby reflecting

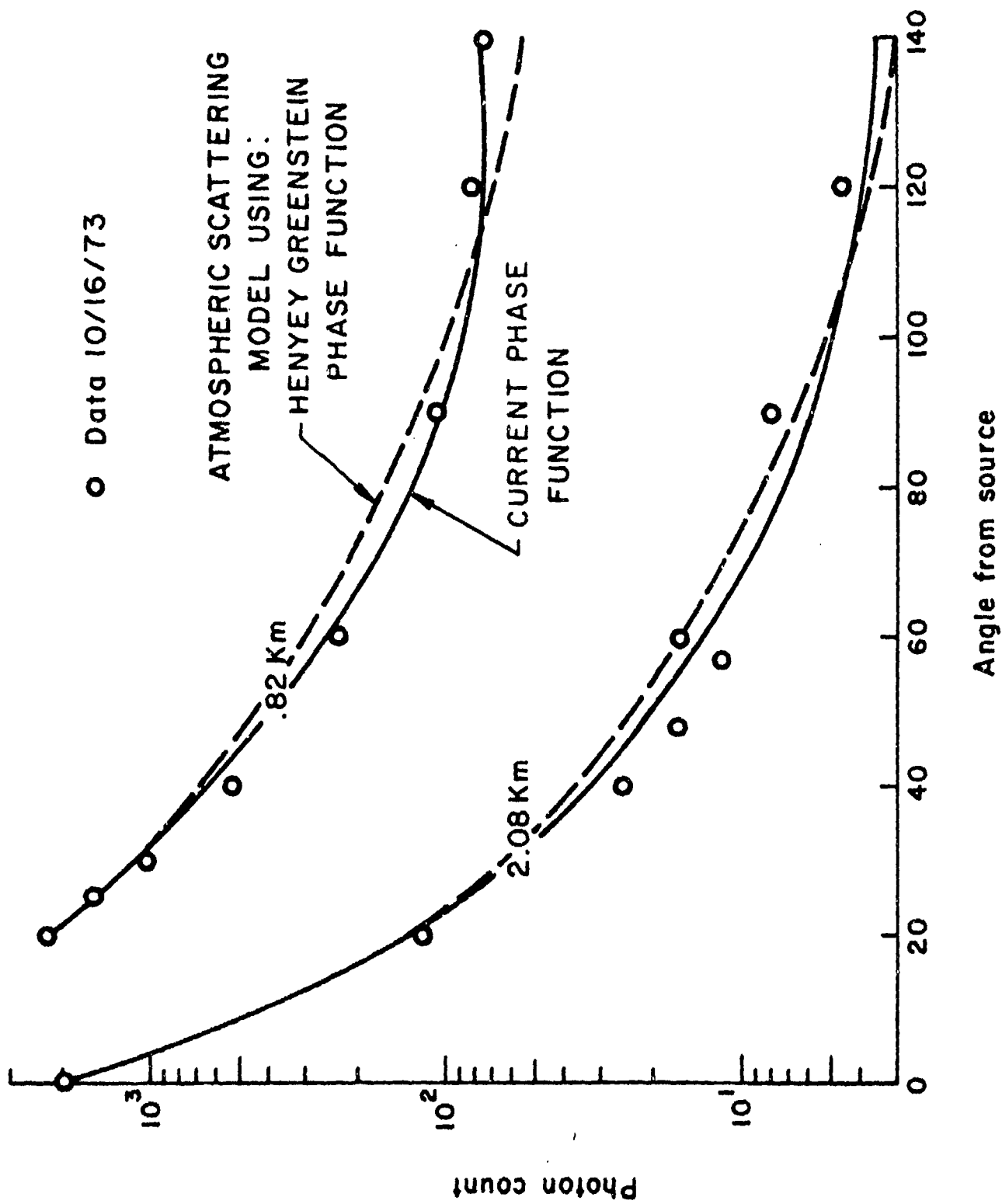


Figure 26. Scattering measurements for two different x locations.

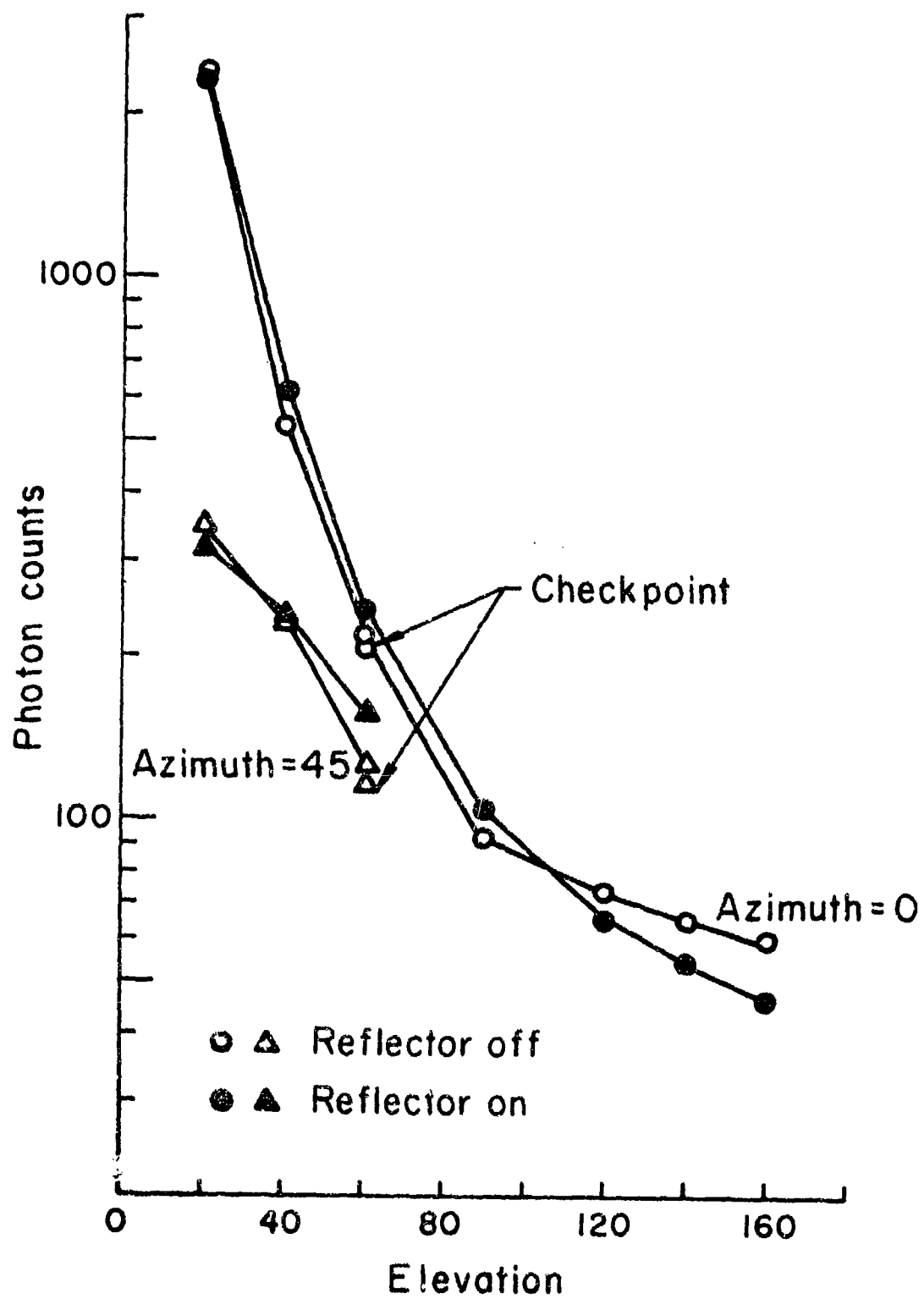


Figure 27. Effects of reflecting additional light into vertical direction.

additional UV light into the horizontal plane in the direction of the detector.

Blocking Experiments

The purpose of this series of experiments was to determine the contributions of various portions of the atmosphere to the signal reaching the receiver. The forward preference of the single scattering phase function played an integral part in these experiments. Unfortunately, the single scattering phase functions in the UV have never been measured. One of the purposes of these measurements was to verify the assumed mathematical formulation of the phase function, which will be discussed in the next section.

The experiments were carried out by using a device which intercepted all of the emitted radiation from the flashlamp up to a given angle from the horizontal, as shown in Figure 28. The interception angle varied from -3° to $+22^{\circ}$ in increments of approximately 2.5° . While zero blocking angle corresponds to the source-to-detector line of sight, negative blocking angles were used because of the finite thickness of the flashlamp. For each blocking angle, the detector angle was varied from 0 to 160° . The overall results of one such survey are shown in Figure 29. It can be seen from Figure 29 that, while the average drop in photon count is nearly 50% for the maximum blocking angle, the decrease is actually less than the decrease associated with rotating the detector an equal number of degrees further away from the source. The 50% overall decrease is also equivalent to moving the detector an additional .25 km away.

Ideally, it would have been desirable to perform the blocking experiments all the way up to a blocking angle of 90° , but a considerably larger and more complicated blocking device would have been required. Nevertheless, a sufficient trend can be seen from Figure 29 to conclude that transmitting and receiving from foxholes or from opposite sides of a hill is certainly possible.

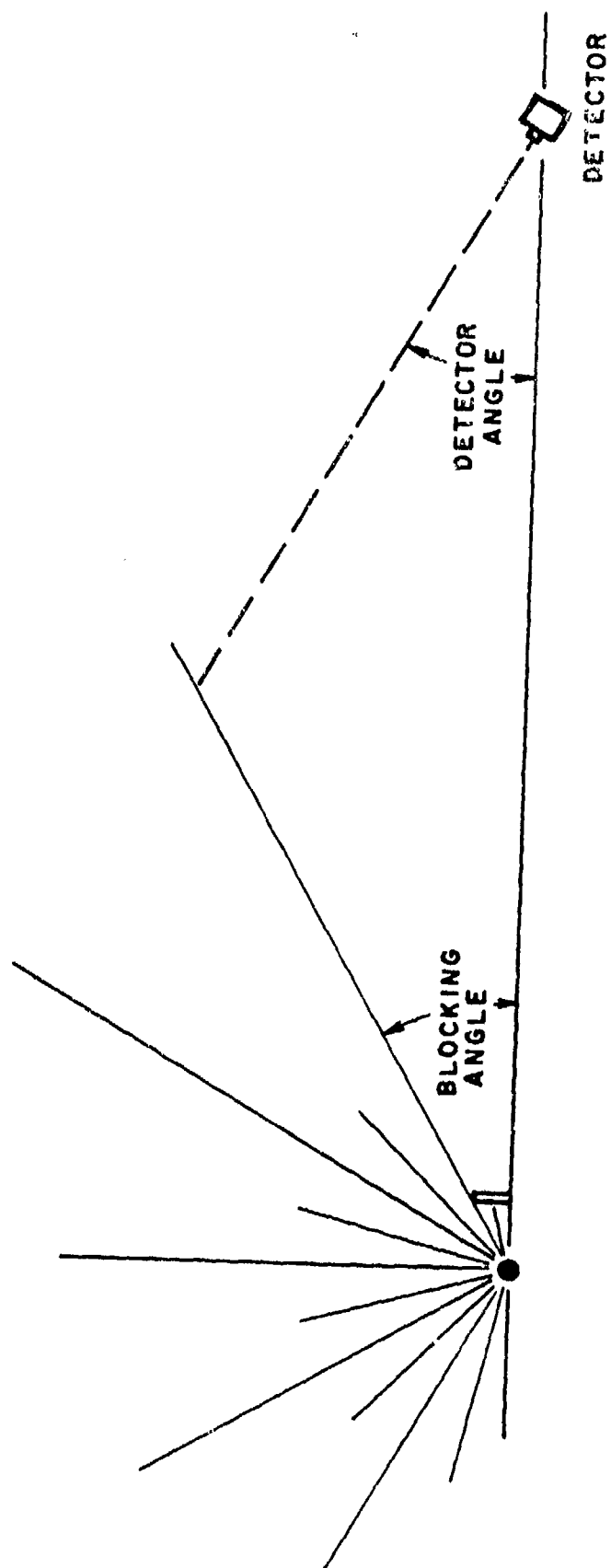


Figure 28. Geometry of blocking experiments.

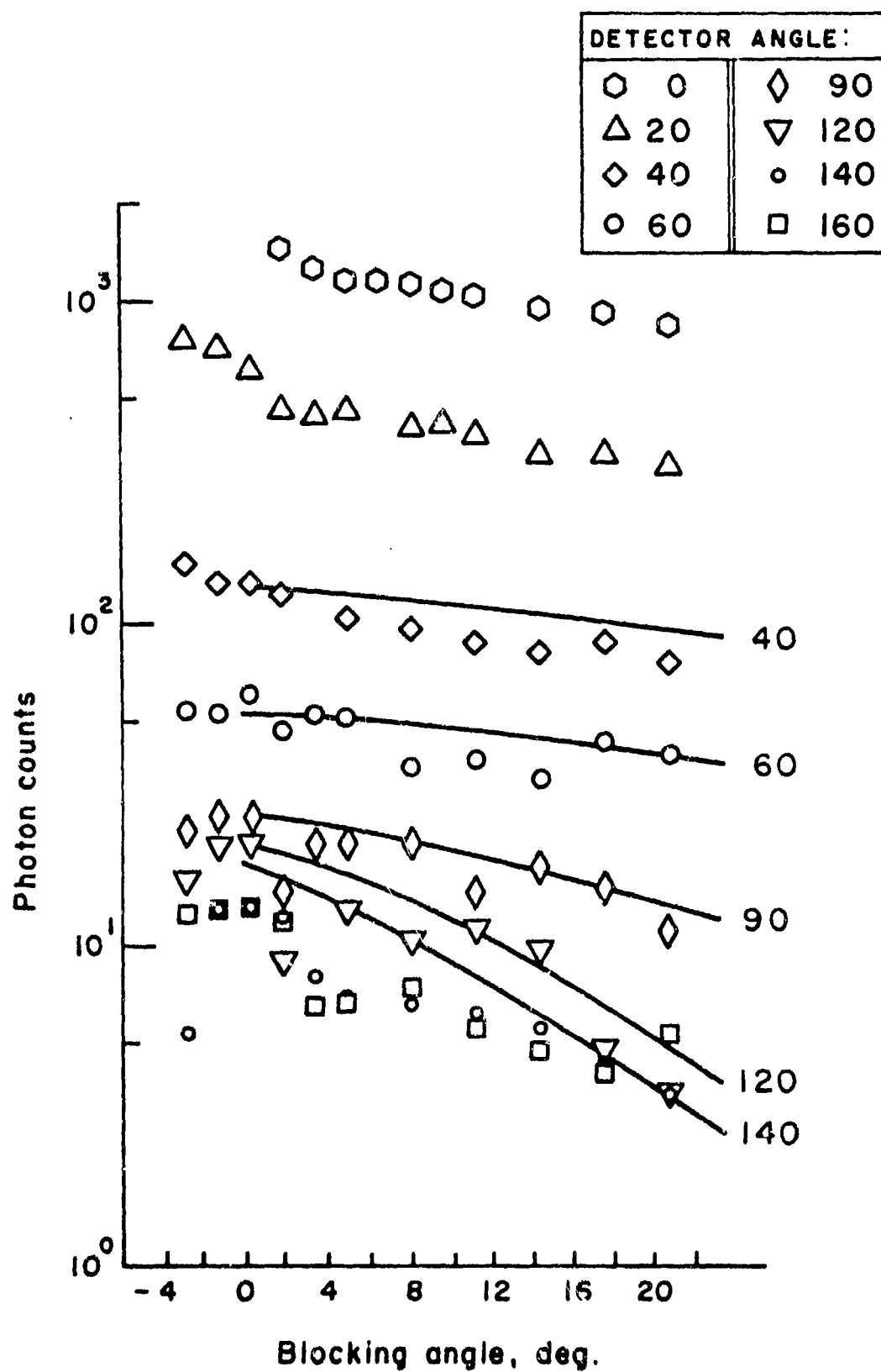


Figure 29. Results of blocking experiments.

Effects of Rain and Scintillation

Due to a fortunate turn of events, it was possible to determine the effects of rain on the atmospheric scattering. Data were obtained for two consecutive days under virtually identical conditions including location, lamp intensity, voltage settings, visibility, temperature, time of day, etc. During the second day, a light misty rain began to fall such that the visibility was reduced to somewhere between 1.5 and 2.0 km. The measured photon counts increased dramatically, as shown in Figure 30. The intensity of the rainfall was such that it took approximately five minutes for a data sheet to become too wet for writing purposes. The increase in signal is significant because it shows that communications using ultraviolet scattering would improve during bad weather while performance of other systems might be degraded.

Scintillation measurements were made on three different occasions, with the results of two shown in Figure 31 and Table 2. It has been found, however, that a good portion of the apparent scintillation shown in Figure 31 is due to electronic noise resulting from inadequate shielding of the detector electronics. It can be seen from Table 2 that scintillation effects increase with distance as might be expected.

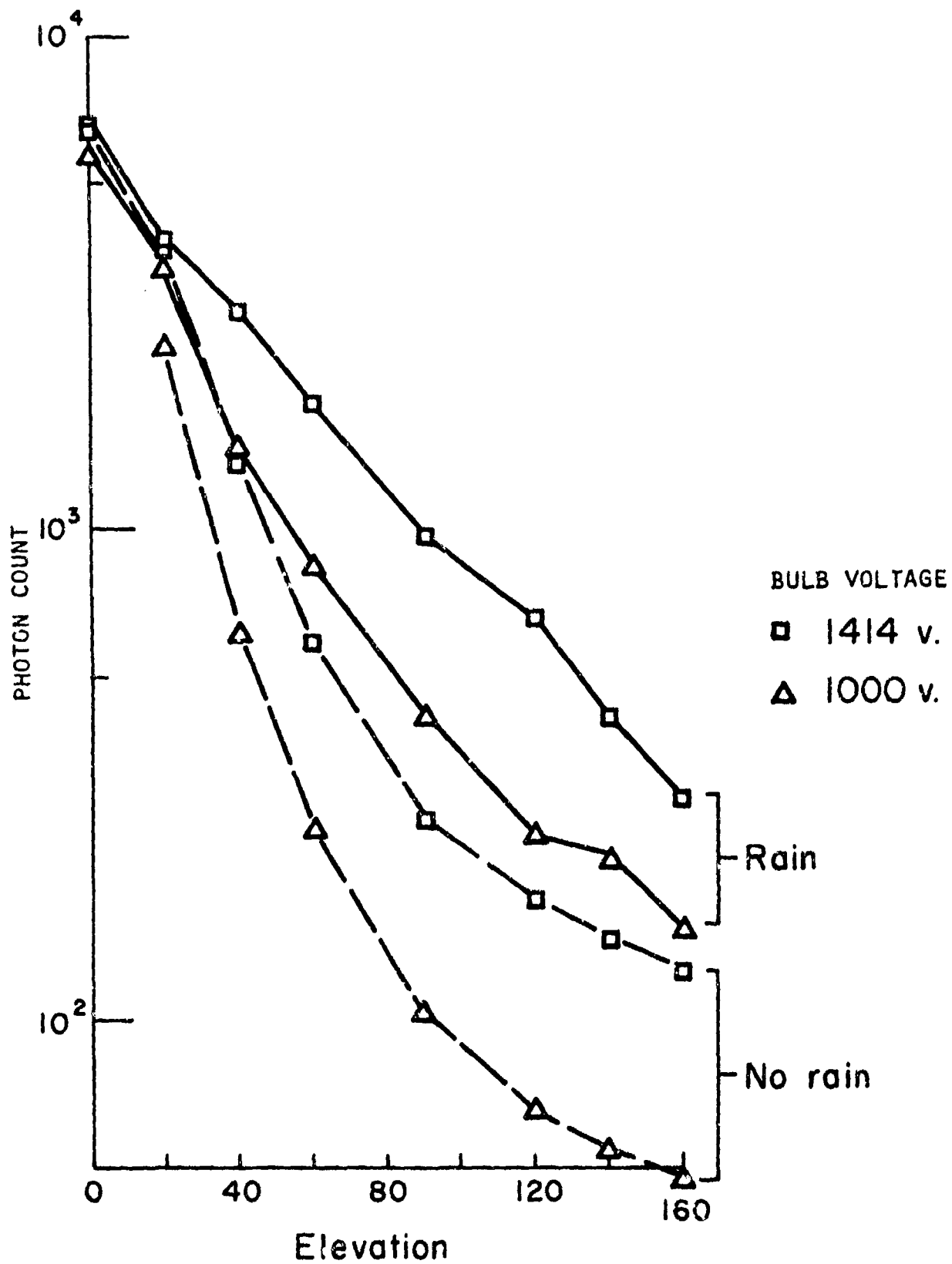


Figure 30. Rain enhancement of scattered radiation.

TABLE 2
VARIATION OF PHOTON COUNT
(PHOTON COUNTS/LAMP-FLASH)

INTENSITY	<u>VARIATION</u>	
	STANDARD DEVIATION	PERCENT
3246	85	2.6
3094	57	1.8
2989	184	6.2
2946	150	5.1
2883	84	2.9
1092	32	2.9
256	16	6.3
152	20	13.2
139	23	16.5
111	11	9.9
92	14	15.2
65	25	38.5

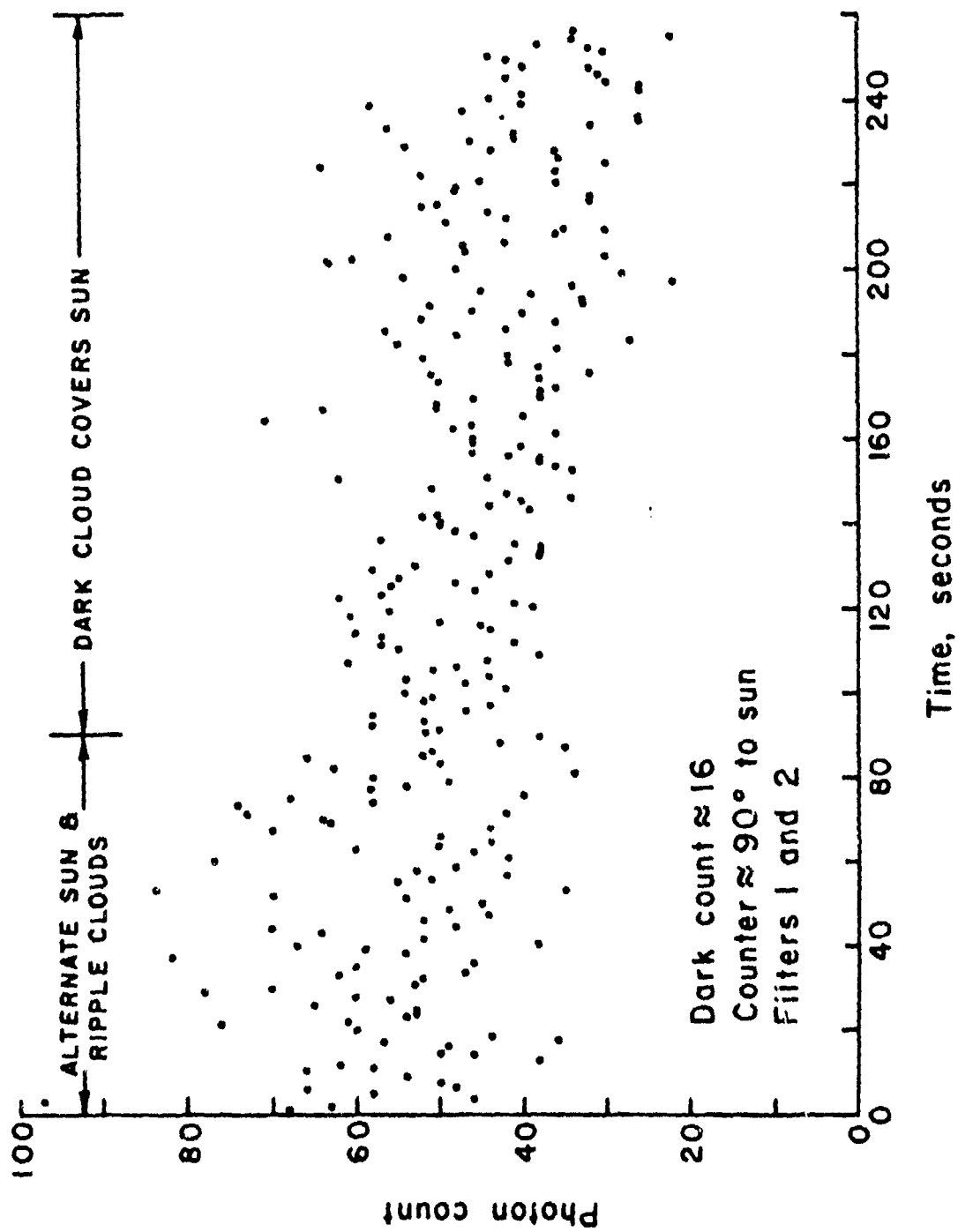


Figure 31. Scintillation measurements of solar background radiation.

IV. THEORETICAL INVESTIGATION

The analysis of atmospheric scattering of UV radiation can be approached in a number of ways. Case and Zweifel (Ref. 4) have investigated the isotropic scattering process in an infinite atmosphere. Levine (Ref. 5) analyzed isotropic scattering in a uniform atmosphere of finite depth. Initially, our efforts were devoted to solving the radiative transfer equation for the more general case of isotropic scattering with absorption and with a finite field of view detector. The results of this initial effort are given in Reference 6. Because of certain limiting assumptions, such as isotropic scattering and weak absorption, the solution to the radiative transfer equation given in Reference 6 does not agree with observed data.

Simplified Scattering Model

The solution of the radiative transfer equation with the additional complication of a nonisotropic scattering function is beyond the scope of the present research. An attempt has been made to construct a simplified semi-empirical model which will accurately predict the observed atmospheric scattering footprints. The basic approach in the development of this semi-empirical model was to account for as many intuitive factors and observed physical phenomena as possible. Only a few constants have been introduced into the model, all of which have some physical significance.

The criteria which have been established for developing the simplified model are given below. Basically, the model should

1. Account for atmospheric absorption of the UV radiation (primarily due to ozone).
2. Account for absorption by the earth's surface.
3. Give higher photon counts at close range as the scattering coefficient is increased. This phenomenon was observed as shown in Figure 30.

4. Give lower photon counts at long range as the scattering coefficient is increased. Although this phenomenon has not actually been observed, it makes sense intuitively that with increased scattering the total path length traveled by a photon in reaching a location far from the source must increase. Since ozone absorption effects are proportional to total path length, the net effect would seem to be a decrease in the number of photons reaching the far location.
5. Utilize a generalized scattering function with arbitrary constants which control the preference for scattering in the forward direction. The surface integral of the function over 4π steradians should be equal to one.
6. Give the correct shape of the atmospheric scattering footprints observed in the field.
7. Give the correct magnitude of the scattering footprints simultaneously at various x locations (see Fig. 23).
8. Give the correct magnitude of photon counts when the source lamp is within the field of view.
9. Give the correct intensities for the blocking experiments.
10. Incorporate the measured field-of-view function.

Assumptions and Model Development

Most of the UV photons reaching a point in the atmosphere are traveling very nearly in a radial direction from the flashlamp. This assumption is easily verified by looking at Figure 26 which shows the angular dependence of the radiation reaching a point in space occupied by the detector itself. Two phenomena are believed to be responsible for this effect. The basic single scattering

phase function is strongly favored in the forward direction. Also, photons which travel more indirect routes are more likely to be absorbed by atmospheric ozone.

The basic geometry used in the model is given in Figure 23. Each point in space is defined by a vector \vec{R} which originates from the flashlamp. Each point in space is also defined by the vector \vec{r} which originates from the detector. In the absence of scattering, the photons which would pass through a small area ΔA , which is perpendicular to \vec{R} , would be equal to

$$\frac{I_0 \Delta A e^{-\sigma_{\text{ABS}} R}}{4\pi R^2}$$

where I_0 is the total number of photons per flash radiated isotropically into space, σ_{ABS} is the absorption coefficient, and R is the length of vector \vec{R} . The term $\Delta A/4\pi R^2$ is, of course, the steradiancy of the area ΔA with respect to the flashlamp.

The fraction of the photons which are scattered before reaching the location at \vec{R} is given by

$$e^{-\sigma_{\text{SCATT}} R}$$

where σ_{SCATT} is the scattering coefficient. Of those which are scattered, η' are scattered into the backward direction and $1 - \eta'$ are scattered into the forward direction. It is assumed that those scattered in the forward direction will still reach the location \vec{R} . Thus, the total number of scattered and transmitted photons reaching the location \vec{R} is given by

$$\frac{I_0 \Delta A e^{-\sigma_{\text{ABS}} R} e^{-\eta' \sigma_{\text{SCATT}} R}}{4\pi R^2}$$

The fraction of photons n' scattered into the backward direction will be determined later by integrating the single scattering phase function over the rearward facing hemisphere.

Of those photons passing through the area ΔA , the fraction scattered over a length Δl (which is parallel to \vec{R}) is, by definition, $\sigma_{SCATT} \cdot \Delta l$. Of those which are scattered, the fraction scattered per unit solid angle in the direction of the detector is given by the single scattering phase function $P(\beta, a)$ where β is the angle the vector \vec{r} makes with the vector \vec{R} as shown in Figure 23, and "a" is a parameter which represents the scattering characteristics of the existing aerosol distribution. Thus, the total number of photons scattered in the volume element $\Delta A \cdot \Delta l$ and heading in the direction of the detector is given by

$$\Delta l \sigma_{SCATT} P(\beta, a) \frac{A_D}{4\pi r^2} \left[\frac{I_0 \Delta A e^{-R(\sigma_{ABS} + n' \sigma_{SCATT})}}{4\pi R^2} \right]$$

where $A_D/4\pi r^2$ is the steradiancy of a detector of area A_D with respect to the scattering volume which is located at a distance r (see Fig. 23).

Not all of the photons leaving the scattering volume will arrive at the detector, due to absorption and scattering. Using the same reasoning as was applied for scattering and absorption along \vec{R} , the fraction of photons lost along \vec{r} would be

$$e^{-r(\sigma_{ABS} + n' \sigma_{SCATT})}$$

Of the photons reaching the detector, only a fraction will actually result in photon counts due to the effects of filter transmission, photomultiplier tube efficiency and geometric losses. All of these effects are accounted for by the field-of-view function $FOV(\theta)$

where θ is the angle between the detector optical axis and the vector \vec{r} in Figure 23. The angular dependence of the field-of-view function for the detector used in this study has been measured and is shown in Figure 15. The total photon count PC due to all volume elements $\Delta V = \Delta A \cdot \Delta l$ in the field-of-view cone of the detector is then given by

$$PC(\gamma) = \iiint \frac{\sigma_{SCATT} P(\beta, a) I_o A_D FVF(\theta) e^{-(R+r)(\sigma_{ABS} + \eta' \sigma_{SCATT})}}{16\pi^2 R^2 r^2} \Delta V \quad (5)$$

Equation (5) is the basic relation used for the simplified scattering model. Because of its complicated form, Eq. (5) has been integrated numerically by computer program. Some of the algebraic relations necessary to integrate the equation are given later in this section.

Single Scattering Phase Function

According to the results of a fairly extensive literature survey, single scattering phase functions in the 2200 to 2800 Å region of the spectrum have never been measured. We therefore initially chose the Henyey-Greenstein phase function given by

$$P(\beta, g) = \frac{1}{4\pi} \frac{1 - g^2}{(1 + g^2 - 2 \cos \beta)^{3/2}} \quad (6)$$

where g is the average value of the cosine of the scattering angle. The Henyey-Greenstein function represents a general family of curves with a forward scattering preference as shown in Figure 32. (Note that the η in Figure 32 is equal to $1 - \eta'$.) These functions were chosen because they exhibit some of the qualitative features of the more realistic Deirmendjian phase functions shown in Figure 33. The Deirmendjian functions were obtained by averaging the Mie scattering functions over polydispersed aerosols. The polydispersed aerosols are classified as haze types,

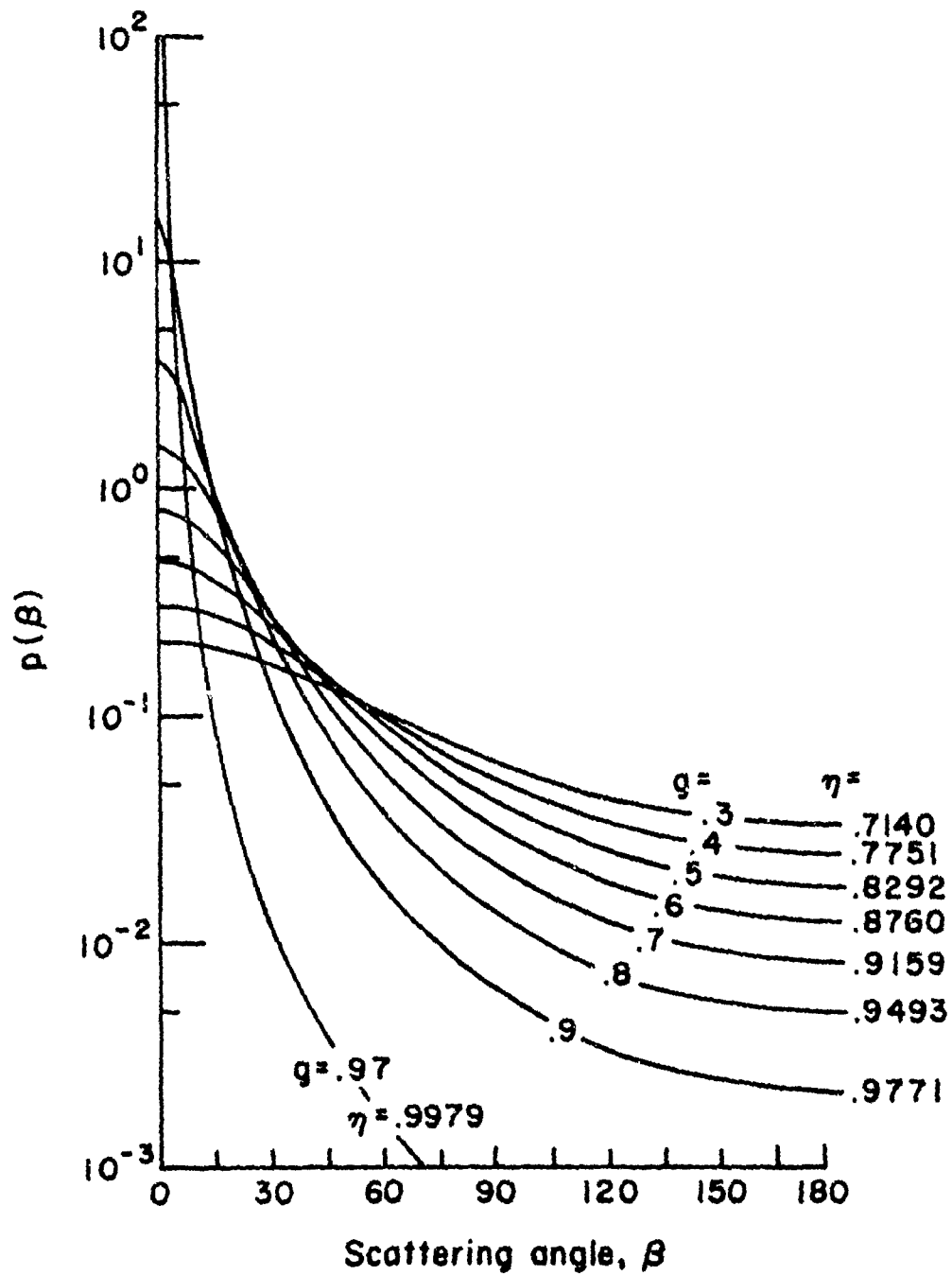


Figure 32. Henyey-Greenstein phase functions.

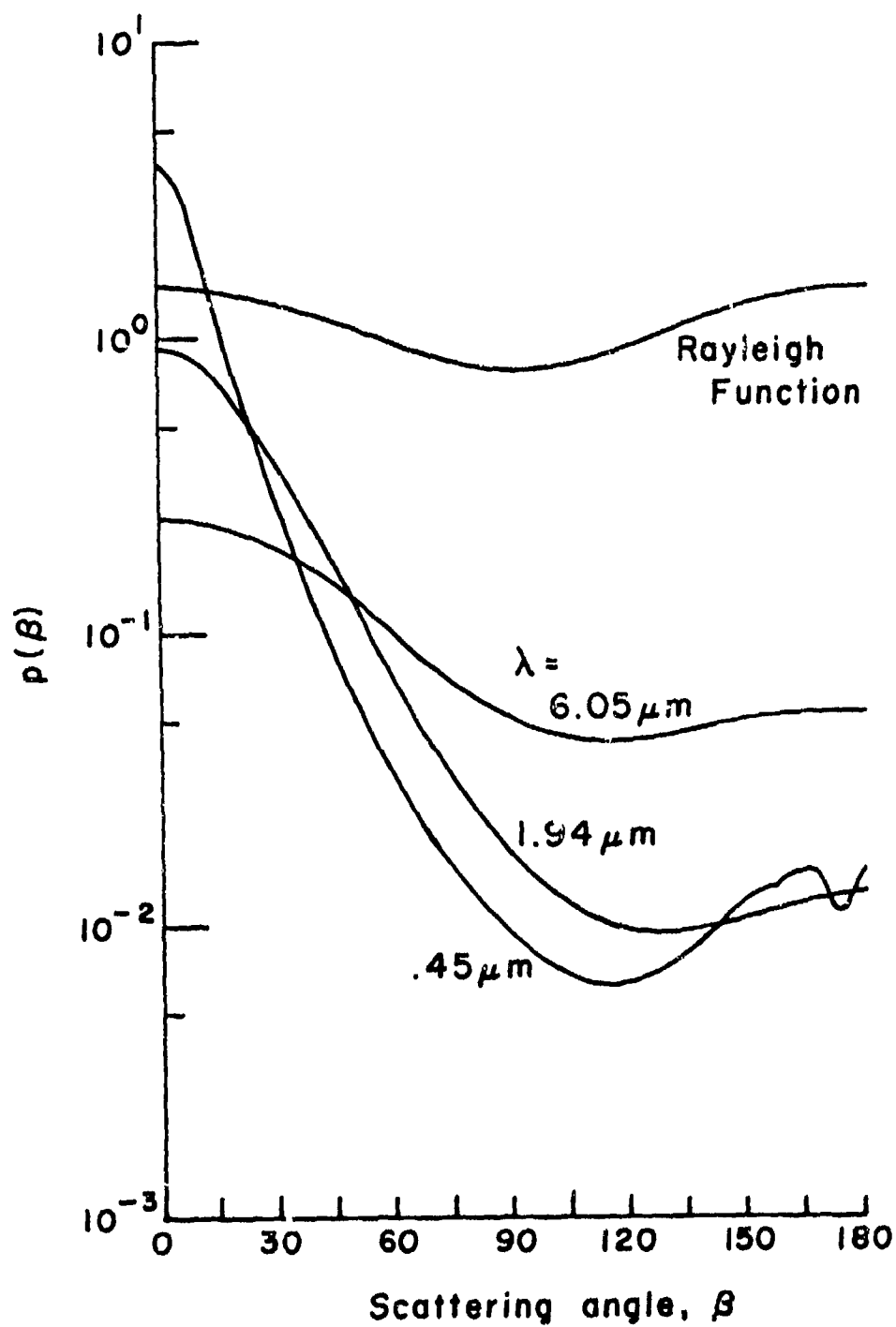


Figure 33. Deirmendjian's phase functions.

as shown in Figure 34 where number density is plotted as a function of particle radius. The Deirmendjian functions shown in Figure 33 correspond to haze type L of Figure 34. The primary qualitative difference between the Henyey-Greenstein and Deirmendjian phase functions is in the region of scattering angles beyond 60° as shown in Figure 35.

Because the Deirmendjian functions exist only in the form of tabulated values for specific wavelengths and haze types, and because they have not been tabulated for wavelengths below 4500\AA , an attempt has been made to modify the Henyey-Greenstein functions to look more like Deirmendjian functions. The modified Henyey-Greenstein functions, which for simplicity will be referred to as the Neer-Sandri functions, are written as

$$P(\beta, g) = \frac{1}{4\pi} \left[\frac{1 - g^2}{(1 + g^2 - 2 \cos \beta)^{3/2}} + \lambda' (3 \cos^2 \beta - 1) \right] \quad (7)$$

where the second term is the second Legendre polynomial. Because the second term is symmetric about $\beta = 90^\circ$, the integral of $P(\beta, g)$ over all solid angles is unchanged. In the same fashion, g , the average value of $\cos \beta$, is also unchanged.

Since the phase function must always be greater than or equal to zero, a value of λ' must be chosen which will ensure that the minimum value of $P(\beta, g)$ is positive. By setting the derivative of Eq. (7) equal to zero, we can express λ in terms of the scattering angle β_0 which corresponds to the minimum value of $P(\beta, g)$.

$$\lambda = \frac{-g(1 - g^2)}{2 \cos \beta_0 (1 + g^2 - 2 \cos \beta_0)^{5/2}} \quad (8)$$

Equation (7) can then be written as

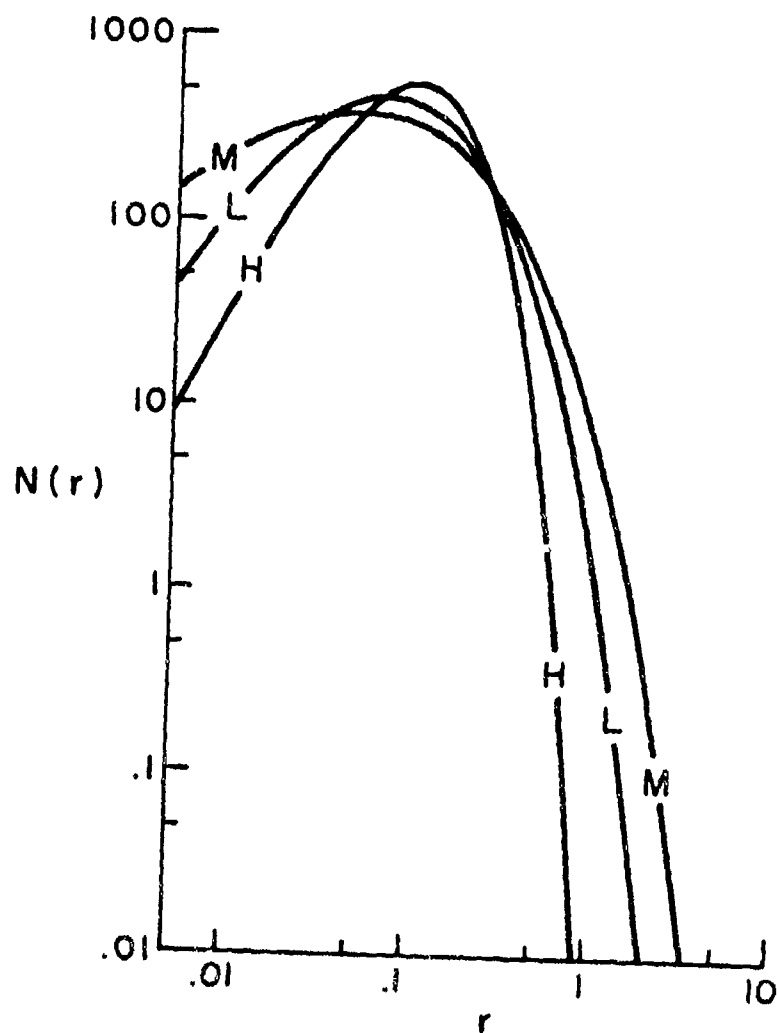


Figure 34. Deirmendjian's haze types. The units for the radius r and for the unit volume in $N(r)$ depend on the particular model. (Reproduced from Reference 8).

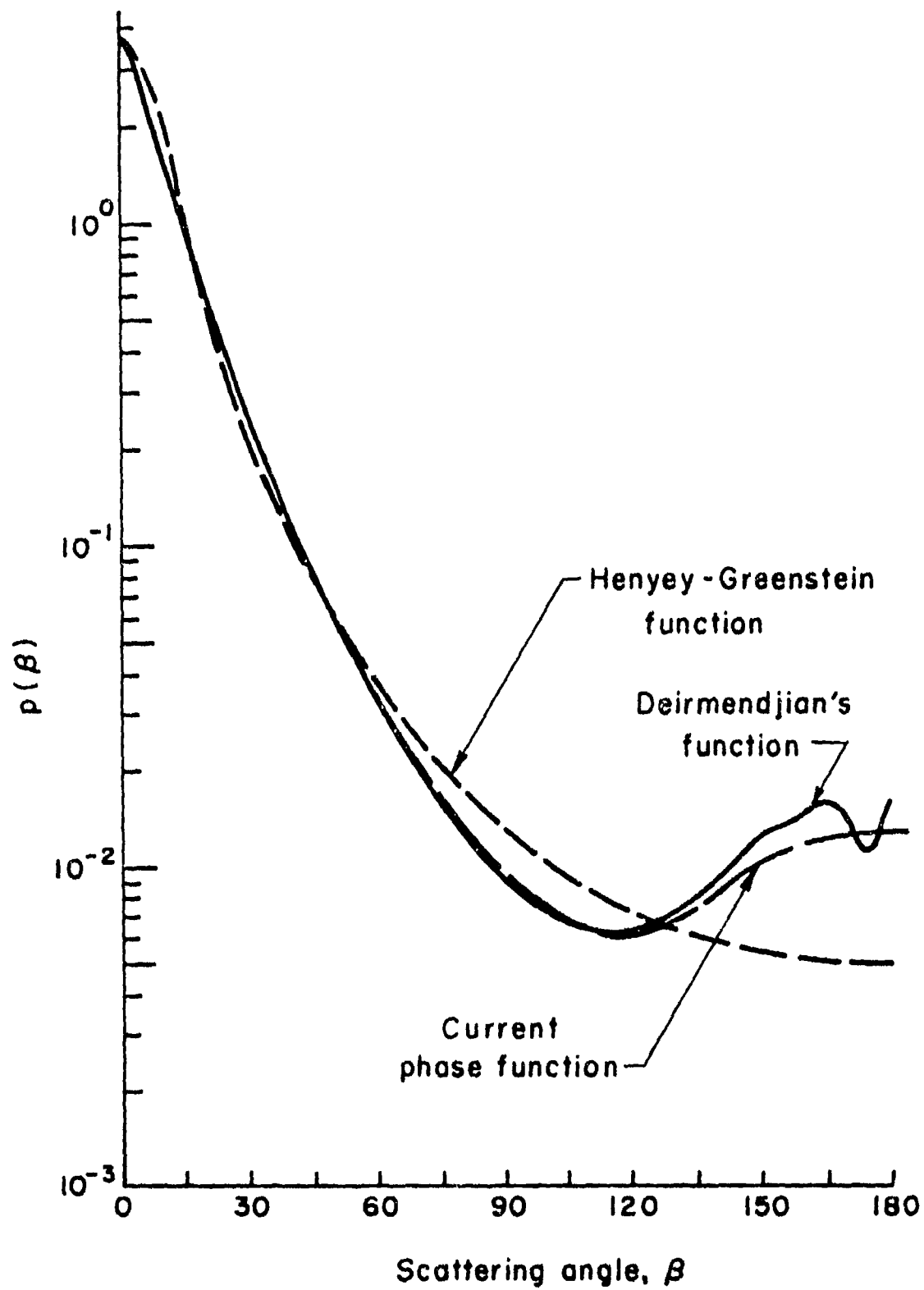


Figure 35. Comparison of various phase functions.

$$P(\beta, g) = \frac{1}{4\pi} \left[\frac{1 - g^2}{(1 + g^2 - 2g \cos \beta)^{3/2}} + \frac{g(1 - g^2)(3 \cos^2 \beta - 1)}{2 |\cos \beta_0| (1 + g^2 + 2g |\cos \beta_0|)^{5/2}} \right] \quad (9)$$

A value of $1/7$ has been chosen for $(\cos \beta_0)$ because it not only guarantees that the phase function will be everywhere positive but also causes the Neer-Sandri function to look like Diermendjian's function as shown in Figure 35.

Multiple Scattering Effects

The atmospheric scattering model described by Eqs. (5) and (9) has one obvious fault. As the distance R increases, the number of times that the average photon has been scattered before reaching that distance increases. The assumption that all photons are traveling parallel to \vec{R} becomes less valid as R increases. Thus, the direction of those photons scattered at \vec{R} will not favor the forward direction as much. In other words, the net effect is that the scattering would appear to become more isotropic as the distance R increases. One way to account for this effect is to allow the effective g value (where g is the average value of the cosine of the scattering angle) to decrease. The effect of decreasing g can be seen in Figure 32 where, as g decreases, the scattering function becomes more isotropic. In order to account for the effects of multiple scattering, the following relation for an effective g value has been assumed:

$$g = g_0 e^{-c_1 \sigma_{\text{SCATT}} R} \quad (10)$$

where g_0 is the actual value for the single scattering phase function and c_1 is a constant describing how fast the effective g value should drop. The functional form of Eq. (10) has been assumed, because for low values of R most of the photons will

not have undergone any scattering prior to reaching R , and hence g should equal g_0 . For very large R , g will go to zero, thus representing totally isotropic radiation. It would not be unreasonable to expect totally diffuse radiation for large values of R , if it were not for the exponential decay with total path length due to ozone absorption.

Since Eq. (10) has been written almost arbitrarily, it is futile to argue the functional dependencies of c_1 . If, however, c_1 could be expressed as a function of g_0 , and g_0 could in turn be measured, Eq. (10) would introduce no arbitrary constants. As it stands now, c_1 and g_0 are both arbitrary constants.

Now that the scattering function has been defined by Eq. (9), it is possible to calculate η' which appears in Eq. (5). η' is defined as that fraction of the scattered light which is scattered into the rearward direction. Hence,

$$\begin{aligned}\eta' &= \int_0^{2\pi} \int_{-1}^0 P(\beta, g) d \cos \beta d\phi \\ &= \frac{1-g^2}{2g} \left[\frac{1}{(1+g^2)^{1/2}} - \frac{1}{1+g} \right] \quad (11)\end{aligned}$$

According to Eq. (10), the effective value of g varies with R . Therefore, at each position R we define a value of η' to represent the average value of backscattering along the path from 0 to R , according to the relation

$$\eta'(R) = \frac{\eta'(g_0) + \eta'(g(R))}{2} \quad (12)$$

Integration of Atmospheric Scattering Relation

The atmospheric scattering model defined by Eqs. (5) and (9) is nearly impossible to integrate in closed form. Consequently, the equation has been integrated numerically by dividing the

field-of-view cone into a finite number of volume elements and summing. When quick calculations are desired, the viewing cone can be divided into circular slices which are perpendicular to the optical axis, as shown in Figure 36. The volume of each slice can be written as

$$\Delta V_1 = \pi(r_1 \tan \theta)^2 \Delta r_1 \quad (13)$$

and the distance R can be expressed in terms of r , AZIM, and ELEV (see Fig. 23) as

$$R = \sqrt{r^2 - 2xr \cos \gamma + x^2} \quad (14)$$

The value of $\cos \beta$ in Figure 23 is found to be

$$\cos \beta = \frac{x[\cos \gamma] - r}{R} \quad (15)$$

where

$$\cos \gamma = \cos(\text{ELEV}) \cos(\text{AZIM}) \quad (16)$$

If more accuracy is desired, the field-of-view cone is divided into spherical volume elements, as shown in Figure 37. The volume of these elements is given by

$$\Delta V_1 = r^2 \sin \theta \Delta r \Delta \theta \Delta \phi \quad (17)$$

where the more general coordinate system shown in Figure 38 must be used to define θ and ϕ . As can be seen from the figure, the z coordinate is defined as the detector line of sight. The flashlamp or source is located a distance \bar{x}_0 from the detector at coordinates x_0, y_0, z_0 and is an absolute angle γ away from the detector line of sight, just as in Figure 23. The centers of the spherical volume elements are defined in spherical coordinates by r , θ , and ϕ . The distance R from the detector to

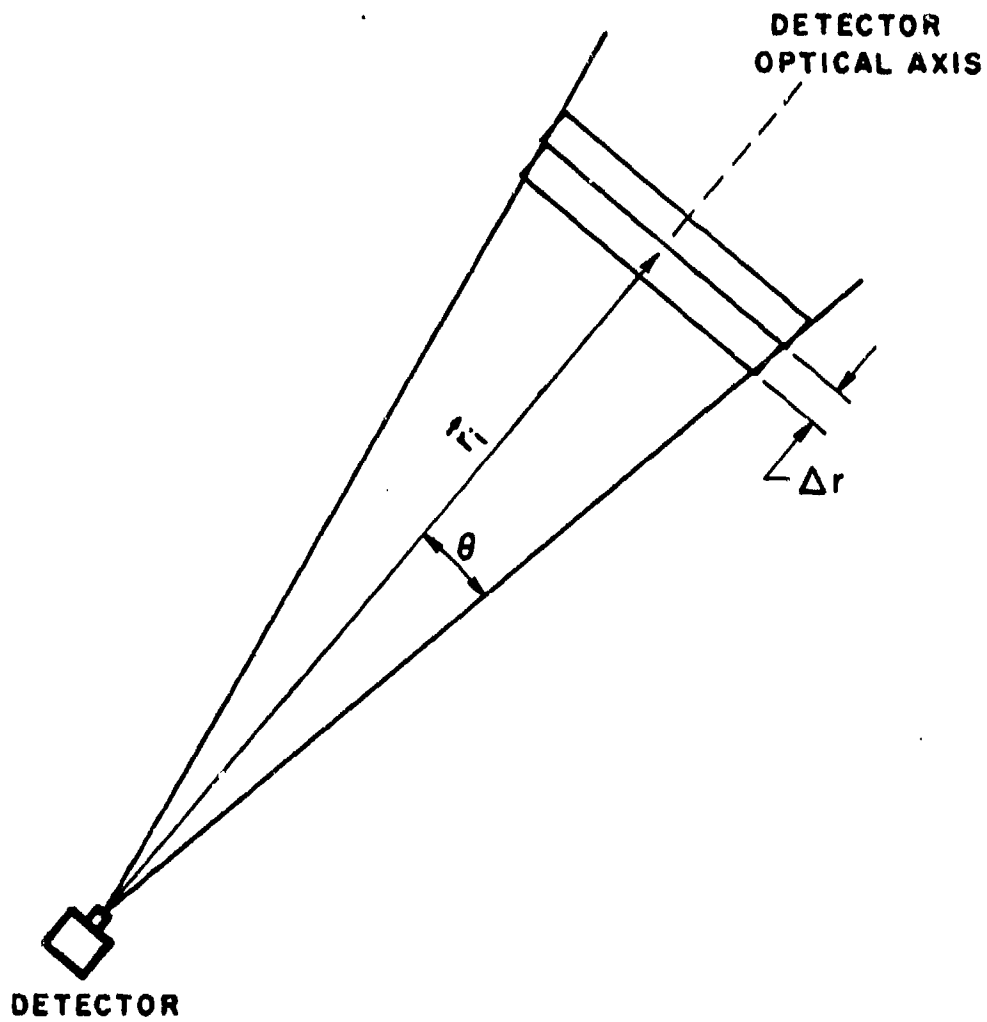


Figure 36. Circular volume elements.

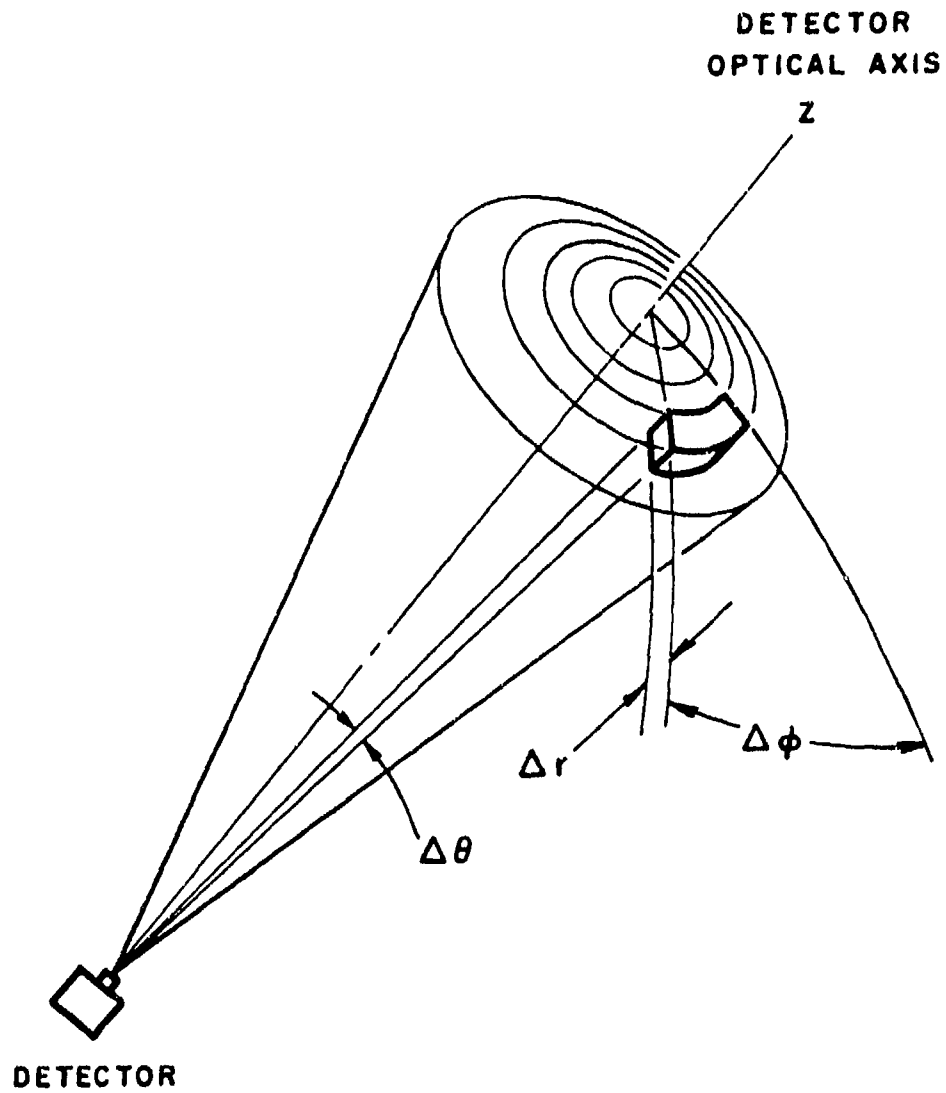


Figure 37. Spherical volume elements.

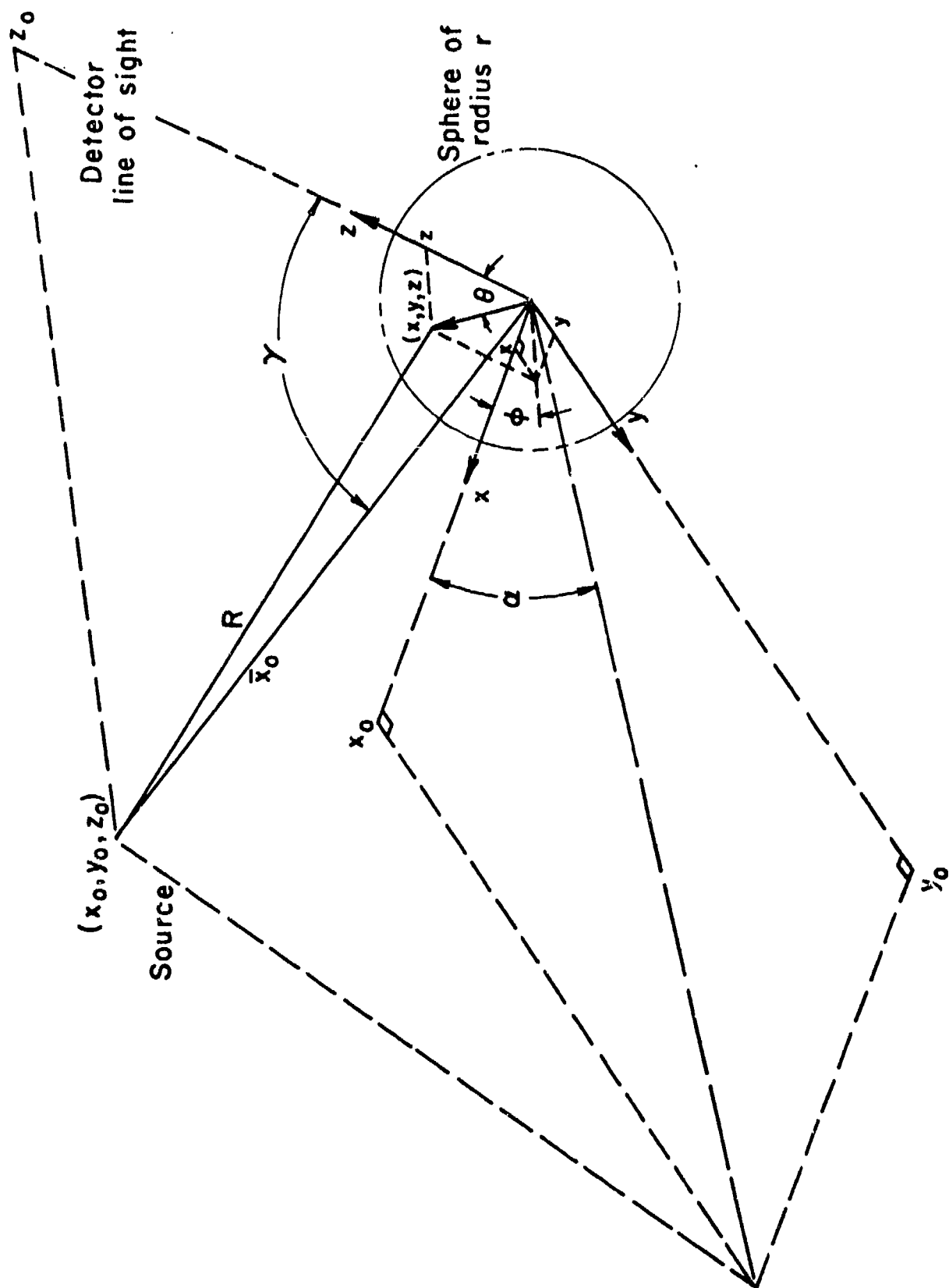


Figure 38. General coordinate system.

a specific spherical volume element is given by

$$R = \sqrt{\bar{x}_0^2 - 2\bar{x}_0 r [\sin \gamma \sin \theta \cos(\alpha - \phi) + \cos \gamma \cos \theta] + r^2} \quad (18)$$

and

$$\cos \beta = \frac{\bar{x}_0 [\sin \gamma \sin \theta \cos(\alpha - \phi) + \cos \gamma \cos \theta] - r}{R} \quad (19)$$

The height above the ground of a volume element can be found if it is assumed that the detector, the lamp, and the y-axis of the detector all lie within the ground plane. In this event, the height z_g is given by

$$z_g = r \cos \theta \sin(\text{ELEV}) - r \sin \theta \cos \phi \cos(\text{ELEV}) \quad (20)$$

The computer program, which numerically integrates Eq. (5), calculates z_g for each volume element and registers a zero if z_g is negative. When the lamp itself is within the field of view, the size of the volume elements greatly decreases in the vicinity of the lamp. Singular point problems are minimized by making sure that the quantity $(4\pi R^3)/3$ is always bigger than the volume element itself.

Regardless of whether the cone slices of the spherical volume elements are used, the computer program input includes σ_{SCATT} , σ_{ABS} , g_0 , c_1 , x , ELEV , AXIM , and I_0 . For comparison with atmospheric scattering data, the value of the attenuation coefficient is measured. In principle, σ_{ABS} should also be determined independently by measuring the ozone concentration. In this study, a value of $\sigma_{\text{ABS}} = .7/\text{km}$ has been assumed, based on tabulated values from Reference 7. The scattering coefficient is then determined from Eq. (4). The number of arbitrary constants is thus limited to g_0 and c_1 . The results of the simplified analyses for $g_0 = .5$ and $c_1 = .3$ are compared with scattering

data in Figure 26. Results are also shown in Figure 26 for the case where the Henyey-Greenstein function (Eq. (6)) is used instead of the Neer-Sandri phase function (Eq. (9)). The $g_0 = .5$ and $c_1 = .3$ case is also compared to the "blocking" experiments in Figure 29. The computer program can be modified to approximate the effects of the blocking experiment for detector angles (see Fig. 28) between 40° and 140° .

The apparent agreement of the simplified model with the field measurements is encouraging. As mentioned earlier, it is possible that some cancellation of error may be involved. However, the agreement between the results predicted by the model and the data of the blocking experiments indicates that we have at least succeeded in predicting which portion of the signal is coming from a particular portion of the field-of-view cone. Also, the agreement obtained at 2.08 km for an angle of 0° (see Fig. 26) is equally encouraging. At 0° , the flashlamp itself is in the field of view, and the photon count is calculated from the sum of Eqs. (2) and (5). If the relative magnitude of scattered and transmitted light calculated was in error, the agreement observed in Figure 26 could not be obtained.

NOTE: CHAPTERS V AND VI HAVE BEEN CLASSIFIED
CONFIDENTIAL AND APPEAR SEPARATELY IN
VOLUME II OF THIS REPORT.

VII. SUMMARY

Voice communication has been accomplished via scattered ultraviolet radiation in the solar blind region of the spectrum. The transmitter is a frequency modulated, high repetition rate, hydrogen-xenon UV flashlamp operating at a carrier frequency of 4810 pulses per second. The receiver is composed of solar blind filters and a rubidium telluride photomultiplier tube. Good quality voice communications have been transmitted around the corner of a building due to pure UV backscattering from atmospheric aerosols. An analysis has been performed which indicates that, with optimization of the various components, a back pack field unit could send and receive voice communication over reasonable distances, which depend on the wavelength, when operating in a purely multidirectional, non-line-of-sight mode. Naturally, heavier systems would have a much longer range. The increase in range which can be accomplished with directional or beamed transmitted UV is not known. A statistical analysis has shown that with a slight modification of the electronic circuitry random background signals due to fires, flares, and other ultraviolet radiation sources can be rejected. The communications system appears to operate better in bad weather due to higher concentrations of atmospheric aerosols.

A high-energy flashlamp and the ultraviolet detector have been used to systematically measure the overall effects of scattering and absorption in the lower atmosphere for light between 2500Å and 2700Å in the solar blind region of the spectrum. The line of sight attenuation coefficients, measured over the .82 and 2.08 km distances between the ground-based flashlamp and detector locations, were found to be consistent with previously published values. The atmospheric scattering footprints obtained by surveying the sky were observed to be symmetric with respect to the angle between the detector optical axis and the detector-to-

flashlamp line of sight. It has been concluded that due to both a strong preference for forward scattering and to an exponential decay with pathlength associated with ozone absorption most of the photons reaching a given point in the atmosphere are traveling very nearly in a radial direction from the flashlamp. A light misty rain was observed to increase the detected radiation by a factor of four.

A simplified theory based on both experimental observation and physical intuition has been developed to model ultraviolet scattering and absorption in the lower atmosphere. The model utilizes the generalized Henyey-Greenstein phase function, modified to more closely resemble Deirmendjian's phase functions for polydispersed aerosols. Multiple scattering effects are modeled by assuming the phase function to become isotropic at large distances from the light source. Two arbitrary constants, introduced to represent the unknown ultraviolet phase function, are chosen to obtain agreement with the magnitude and angular dependence of measured radiation at a given source-to-detector distance. Simultaneous agreement between theory and experiment for another source-to-detector distance, as well as for other related experiments, tends to validate the choice of constants as well as the overall model.

VIII. REFERENCES

1. A. Dutsch, Arch. Meteorol. Geophys. Bioklimator, Vol. All, p. 240, 1959.
2. E. Stokes Fishburne, "The Design and Construction of a Solar Blind Missile Launch Detector," Grumman Aerospace Corp., Bethpage, NY, January 1973.
3. W.A. Baum and L. Dunkelman, "Horizontal Attenuation of Ultraviolet Light by the Lower Atmosphere," J. Optical Society of America, Vol. 95, No. 3, 1955.
4. K. Case and P. Zweifel, *Linear Transport Theory*, Addison-Wesley, Reading, Mass., 1967.
5. P.H. Levine, "Diffuse Radiation from a Point Source in a Planetary Atmosphere," Astrophysics Research Corp., Los Angeles, CA, June 1955.
6. E. Stokes Fishburne and Guido Sandri, "An Investigation of Ultraviolet Communication Techniques," Aeronautical Research Associates of Princeton, Inc., Tech. Memo. No. 75-3, July 1975.
7. L. Elterman, "Rayleigh and Extinction Coefficients to 50 km for the Region 0.27μ to 0.55μ ," Applied Optics, Vol. 3, No. 10, pp. 1139-1147, 1964.
8. D. Diermendjian, *Electromagnetic Scattering on Spherical Polydispersions*, American Elsevier Publ. Co., New York, 1969.